

GHASS CRUISE REPORT

Stephan Ker (Project leader and Leg 1 chief scientist)

Vincent Riboulot (Leg 2 chief scientist)

GHASS cruise team

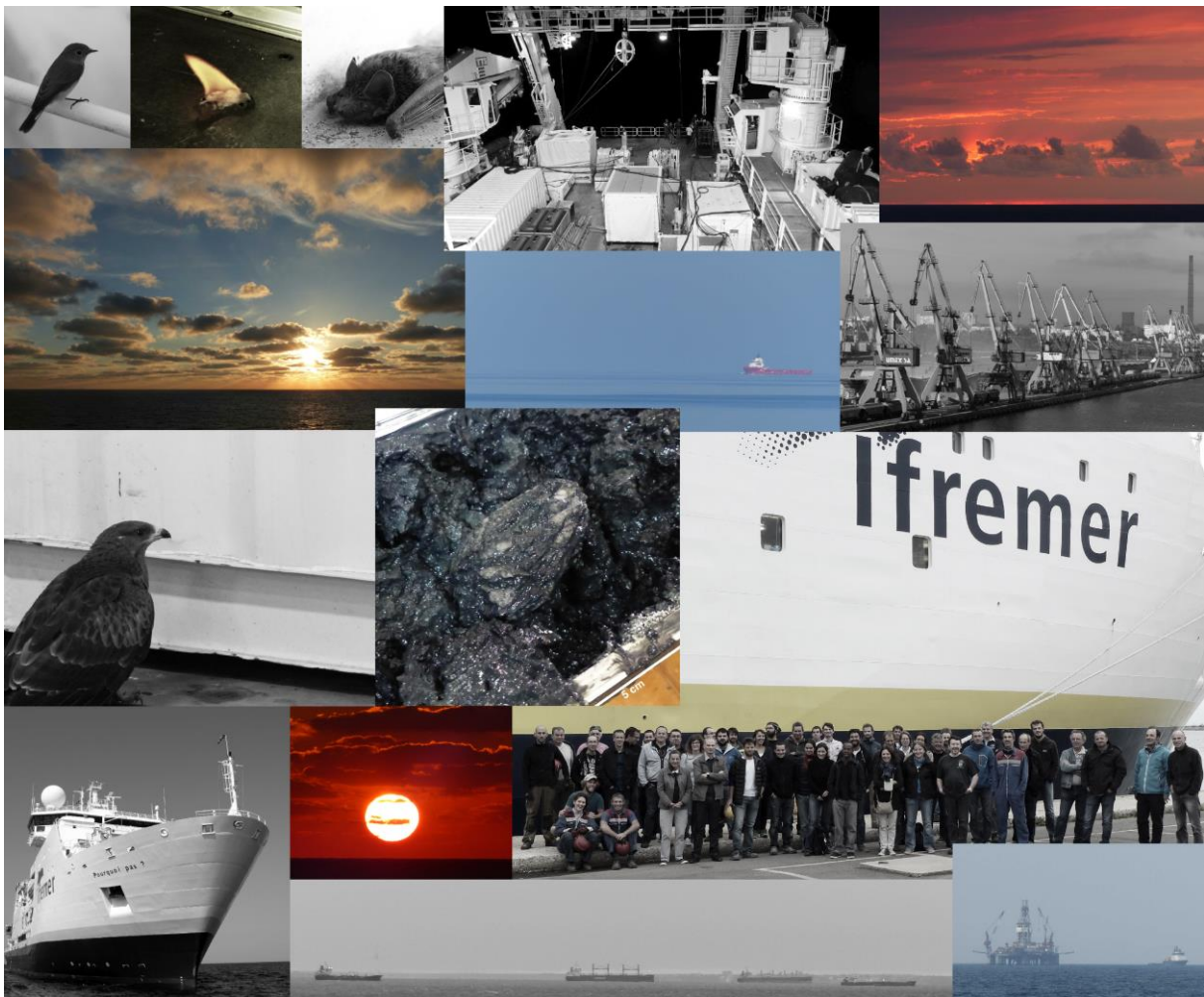


Table of contents

I. SUMMARY	3
II. THE SCIENTIFIC TEAM.....	3
II.1. First Leg scientists.....	3
II.2. Second Leg scientists.....	4
III. RESEARCH PROGRAM OF THE GHASS CRUISE	5
IV. NARRATIVE OF THE CRUISE.....	7
IV.1. Leg 1 narrative	7
IV.2. Leg 2 narrative	8
V. GEOPHYSICAL DATA ACQUISITION	11
V.1. Bathymetry and Seafloor reflectivity	11
V.2. Sub-bottom Profiler	13
V.3 Water column acoustic acquisition	14
V.4. High Resolution Seismic Acquisition	16
V.4. SYSIF deep-towed seismic acquisition.....	19
VI. <i>IN SITU</i> DATA ACQUISITION	23
VI.1. <i>In Situ</i> geotechnical and acoustic soundings (Penfeld penetrometer).....	23
VI.2 Pore pressure and temperature measurements with the Ifremer piezometer.....	28
VI.3. Coring	34
VI.4. Heat flux measurements	38
VI.5. Anitra deployment	39
VI.5. Water Column Survey – CTD-rosette	40
VII. ANALYSIS ON PISTON CORES.....	43
VII.1. Geotechnical and acoustic measurements on piston cores	43
VII.2. Geochemistry analysis	44
VIII. REFERENCES	50

I. SUMMARY

The objectives of the GHASS (Gas Hydrates, fluid Activities and Sediment deformations in the western Black Sea) cruise are twofold but interconnected. The first aim is to study the dynamics of gas hydrates and free gas associated with geological and climate processes. The second aim is to identify the factors at the origin of observed sediment deformations and submarine landslides in two areas in the Romanian sector of the Black Sea. For the cruise we use quantitative approaches based on multidisciplinary studies (geochemistry, geology, geophysics and geotechnics). Gas hydrates and free gas were detected using surface and deep-towed HR seismic (SYSIF) techniques and by performing in situ geotechnical and acoustic measurements using the Ifremer penetrometer (Penfeld). Dynamics of gas hydrate and free gas were evaluated based on geochemical analysis of pore fluids but also by carrying out *in situ* geotechnical measurements and long-term monitoring (several years) of few key sites with pore pressure and temperature measurements. The deformation and submarine landslides associated with gas hydrates, free gas and/or the Danube canyon activities were also studied by using advanced geotechnical technologies and detailed sedimentological studies on sediment cores. One of the main results of the GHASS cruise was to recover gas hydrates from coring for the first time in the Romanian sector of the Black Sea.

II. THE SCIENTIFIC TEAM

II.1. First Leg scientists

Name	Surname	Expertise	Scientific Institute
Colin	Florent	Geophysics	Ifremer
Crozon	Jacques	Geotechnics	Ifremer
Dupont	Pauline	Geophysics	Ifremer
Gaillot	Arnaud	Bathymetry	Ifremer
Hamon	Mathieu	Geophysics	Ifremer
Ker	Stephan	Chief Scientist /Geophysics	Ifremer
Marsset	Bruno	Geophysics	Ifremer
Ogor	André	Acoustics	Ifremer
Riboulot	Vincent	Geology	Ifremer
Roudaut	Mickael	Geotechnics	Ifremer
Ruffine	Livio	Geochemistry	Ifremer
Scalabrin	Carla	Acoustics	Ifremer
Thomas	Yannick	Geophysics	Ifremer
Dutu	Florin	Geology	GeoEcoMar
Zander	Timo	Geophysics	Geomar
Badhani	Shray	Geophysics	Geomar
Sauvin	Guillaume	Geophysics	NGI
Cabello	Patricia	Geology	University of Barcelona

Table 1: Participants of Leg 1.

II.2. Second Leg scientists

Name	Surname	Expertise	Scientific Institute
Apprioual	Ronan	Geotechnics	Ifremer
Bermell	Sylvain	GIS	Ifremer
Boullart	Cedric	Geochemistry	Ifremer
Boissier	Audrey	Geochemistry	Ifremer
Cattaneo	Antonio	Geology	Ifremer
Chéron	Sandrine	Geochemistry	Ifremer
Crozon	Jacques	Geotechnics	Ifremer
Donval	Jean-Pierre	Geochemistry	Ifremer
Dupont	Pauline	Geophysicis	Ifremer
Garziglia	Sébastien	Geotechnics	Ifremer
Guyader	Vivien	Geochemistry	Ifremer
Jorry	Stephan	Geology	Ifremer
Jouet	Gwenael	Geology	Ifremer
Ker	Stephan	Geophysics	Ifremer
Marsset	Tania	Geology	Ifremer
Ogor	André	Acoustics	Ifremer
Payo Payo	Marta	Geology	Ifremer
Riboulot	Vincent	Chief Scientist / Geology	Ifremer
Roubi	Angélique	Geology	Ifremer
Roudaut	Mickael	Geotechnics	Ifremer
Rovere	Mickael	Geology	Ifremer
Ruffine	Livio	Geochemistry	Ifremer
Scalabrin	Carla	Acoustics	Ifremer
Silva-Jacinto	Ricardo	Geology	Ifremer
Toucanne	Samuel	Geology	Ifremer
Woerther	Patrice	Geotechnics	Ifremer
Ion	Gabriel	Geology	GeoEcoMar
Popa	Adrian	Geology	GeoEcoMar
Deusner	Christian	Geochemistry	Geomar
Kossel	Elke	Geochemistry	Geomar
Cerdà	Marc	Geology	University of Barcelone

Table 2: Participants of Leg 2

III. RESEARCH PROGRAM OF THE GHASS CRUISE

“Gas hydrate dynamics, fluid activities and sediment deformations”

Gas flares along the border of Gas Hydrate Stability Zones (GHSZ) and Gas Hydrate Occurrence Zones (GHOZ) have been reported in many areas around the world and mainly in the Black Sea [see for instance Naudts et al., 2006, Klaucke et al., 2006, Nikolovska et al., 2008] and more recently offshore Svalbard [see for instance Westbrook et al., 2009]. Naudts et al. [2006] suggested that gas hydrates play the role of buffer for the upward migration of free gas and thus prevent the rise of gas bubbles into the water column. Westbrook et al. [2009] propose that in addition to the buffer role of gas hydrates, gas vents may be amplified by the temperature changes recorded during the last 3 decades. Westbrook et al. [2009] suggest that gas flares are a direct indication of gas hydrate dissociation related to ongoing climate changes. These two previous interpretations are based mainly on seismic profiles and water column data acquisition without any long-term observation and quantitative measurements. In this work, we propose to study the link between gas hydrate dynamics and fluid activities in the Romanian sector of the Black sea by carrying-out long-term monitoring of pore pressure and temperature in the upper 15 m of sediments and at the border of the GHOZ. The main aim is to identify any possible link between temperature changes and fluid pressures which could be the result of gas hydrate dissociation.

The possible link between free gas and gas hydrate dynamics and sediment deformations and submarine landslides is also an important question for the GHASS cruise. For the last 3 decades, several authors have raised serious concerns regarding the possible link between gas hydrate and submarine slope failures. McIver [1982] was among the first authors to speculate on this possible link. In the McIver conceptual model, the excess pore pressure generated by hydrate dissociation and the sediment shear strength decreases (lost of hydrate playing the role of cementing agent between sediment grains) are the two key factors in the slope failure mechanism. The Romanian sector of the Black sea seems to be a perfect site to carry out this type of slope stability analysis by using multidisciplinary studies and approaches.

“Assessment of the environmental impacts of the exploitation of deep sea methane hydrates”

Several international projects deal with gas hydrates as a potential source of energy. The German project SUGAR aims to produce natural gas from marine methane hydrates and to sequester carbon dioxide (CO₂) [Wallmann and Bialas, 2009]. The Japanese hydrate drilling project is located in the Nankai Trough region along the south-eastern margin of Japan. This project, now in its second phase (2009-2015), aims to develop two offshore production tests [Masuda et al., 2009]. For the Mallik site, in Canada’s Mackenzie Delta, a production test was already been performed in 2007-2008 and demonstrated the feasibility of methane production from methane hydrate by depressurization [Dallimore et al., 2008]. Several other projects are under development or have already been developed in India, China and South Korea. In the United States, significant accumulations of methane hydrate occur in the Gulf of Mexico, off the Pacific and Eastern seaboard, and on the Alaska North Slope. However, the environmentally and economically sustainable production of methane from methane hydrate in these locations has not yet been achieved [DOE report, 2010].

It is essential to evaluate the environmental impacts of this type of hydrate production project. One of the main issues regarding gas hydrate production is the mechanical behaviour of gas hydrate bearing sediment and its evolution due to gas hydrate dissociation during the production phase. How, the sediment partially saturated by gas hydrates, will behave once the gas hydrate is dissociated or dissolved? What will the consequences be in terms of sediment deformations and submarine landslides? The proposed scientific cruise will try to provide the necessary information and data to assess such environmental impacts of the exploitation of deep sea methane hydrates.

The Romanian sector of the black sea: geological setting

The Black Sea is a land-locked basin of ca 432.000 km², connected to the Mediterranean Sea by the Bosphorus Strait, and originated from back-arc extension associated with the Mesozoic northward subduction of the Thetian plate [Robinson et al., 1995]. The north-western Black Sea, infilled by thick sedimentary successions of up to 19 km since the Cretaceous, is the main depocentre for sediment supply from Central Europe via the Danube River and from Eastern Europe through the Ukrainian rivers Dniepr, Dniestr and Southern Bug [Robinson et al., 1995]. These sediment supplies contributed to the shaping of the north-western Black Sea margin from the coastal area, marked by deltaic deposits, down to the deep basin, where large deep-sea fan complexes including the Danube deep-sea fan formed [Wong et al., 1994; Popescu, 2002; Lericolais et al., 2012].

The continental shelf is particularly wide in the north-western sector of the black Sea (up to 170 km off the Dniepr River). The shelf-break is located at water depths of -120 to -140 m southward of the Danube Canyon, and up to -170 m northward of the canyon possibly due to recent faulting. A relatively steep slope (2.5%) lies between the shelf-break and the flat abyssal plain (2200 m water depth) [Popescu et al., 2007]. The continental slope is dissected by numerous canyons which commonly stop at the shelf-break with the exception of the Danube Canyon which deeply incised the shelf for 26 km landward (up to -110 m water depth). The Danube Canyon acted as a major gateway for the sediment transfer towards the deep Black Sea [Popescu et al., 2004].

In addition to terrigenous supply, river inputs constantly introduced high amounts of organic-rich material into the Black Sea. The specific history of the Black Sea, including times of periodical sea bottom anoxia, created particularly favourable conditions for the decomposition of organic matter and for gas generation. Geophysical-based studies reveal free gas in sediments (inferred from BSR, i.e. bottom-simulating reflections) and gas escape in the water column. In detail, the distribution of the gas facies shows (i) major gas accumulations close to the seafloor in the coastal area and along the shelfbreak, (ii) ubiquitous gas migration from the deeper subsurface on the shelf and (iii) gas hydrate occurrences on the lower slope (below 750 water depth) [Popescu et al., 2007].

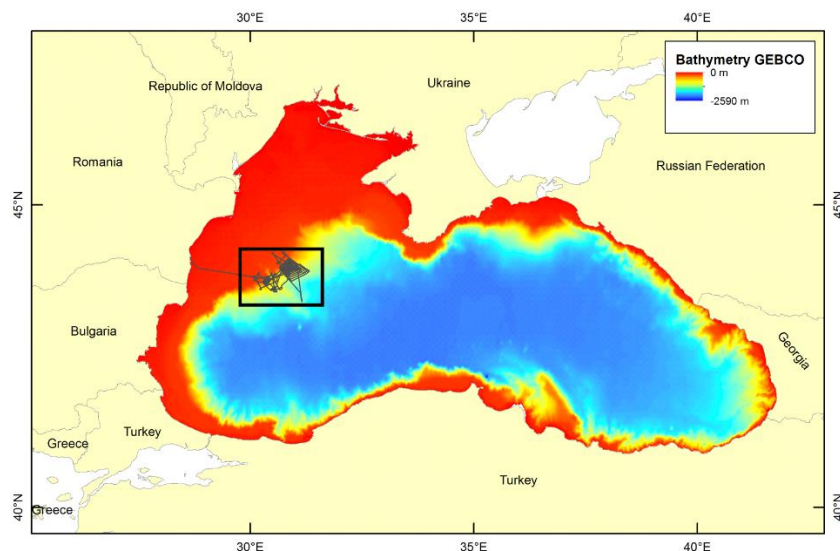


Figure 1: Regional settings of the Black Sea with main on land drainage systems and offshore rim currents. Red arrows point out major sediment discharges at river mouth. Yellow boxes represent the three study areas of the GHASS cruise, namely from north to south: Area N, Area C, Area S.

IV. NARRATIVE OF THE CRUISE

IV.1. Leg 1 narrative

The first leg was dedicated to geophysical acquisition. This leg aims to acquire the bathymetry of studied areas, to perform high resolution sea surface acquisition and very high resolution deep-towed seismic acquisition. Deployment and recovery of piezometers were undertaken as well as the deployment of the ANIITRA station.

The acquisition of the first leg is the following:

- 72 hours of bathymetry acquisition (300km²), water column acoustics and sub-bottom profiler acquisition (22% of the leg),
- 92 hours of HR seismic acquisition split into two sequences, 21 profiles with a total length of 320 km (27% of the leg),
- 120 hours of SYSIF deep-towed acquisition in three dives, 30 profiles with a total length of 300 km,
- 12 hours for the deployment/recovery of piezometers and ANIITRA (3%)
- 12 hours for water column acoustic acquisition (3%)

The acquisition phases conducted during the first leg are described in Table 2.

Date	Hour	Area	Phase
01/09/2015	05:30:00		Transit
01/09/2015	12:54:34	S	Piezometer recovery
01/09/2015	13:28:46		Transit
01/09/2015	14:35:29	S	ANIITRA deployment
01/09/2015	16:40:07		Transit
01/09/2015	18:36:23	N	Bathymetry
03/09/2015	13:01:19	N	Failure of the second piezometer recovery
03/09/2015	15:34:01	N	HR seismic acquisition
05/09/2015	15:56:32	N	Deep-towed seismic
07/09/2015	20:41:33		Transit
07/09/2015	21:34:36	N	Deployment of short term piezometer
08/09/2015	02:06:45		Transit
08/09/2015	03:48:32	S	Bathymetry
08/09/2015	21:53:51	S & N	HR seismic acquisition
10/09/2015	18:04:02		Transit
10/09/2015	18:30:48	S	Deep-towed seismic
11/09/2015	13:50:34		Transit
11/09/2015	15:24:25	N	Piezometer site test
11/09/2015	16:40:33		Transit
11/09/2015	17:45:17	S	Bathymetry
12/09/2015	04:25:33		Transit
12/09/2015	05:45:00	N	Deployment of short term piezometer
12/09/2015	07:07:59		Transit
12/09/2015	08:40:48	N	Deep-towed seismic
14/09/2015	06:39:57		Transit
14/09/2015	07:49:40	N	Deployment of short term piezometer
14/09/2015	10:49:18	N	Water Column Acoustics
14/09/2015	21:03:43		Transit

Table 3: Course of the Leg 1.

IV.2. Leg 2 narrative

The second leg was dedicated to *in situ* acquisition performed with a range of corers, the Penfeld penetrometer, piezometers and CTD probe. This leg aims to collect cores for sedimentological description, geochemical analysis of pore water, physical property analysis and geotechnical *in situ* measurements.

During the second leg, we performed:

- water column acoustic studies
- 12 dives of the Penfeld penetrometer
- 15 Calypso cores
- 12 interface cores
- 3 gravity cores
- 6 piezometer deployments (2 long-term and 4 short term)
- 2 CTD dives

The acquisition phases conducted during the second leg are described in table 3.

Date	Hour	Latitude	Longitude	Phase Name	Depth (m)
16/09/2015	05:55:07	N 44° 5,28431'	E 28° 42,60137'	Transit	
16/09/2015	14:15:56	N 44° 5,14765'	E 30° 47,93308'	Calypso CS01	244
16/09/2015	16:50:10	N 44° 5,03028'	E 30° 48,32424'	SMF-SDS	267
16/09/2015	18:22:00	N 43° 58,60489'	E 31° 1,84787'	Penfeld CPT01	831
17/09/2015	06:30:32	N 43° 57,85532'	E 31° 3,70837'	SMF-SDS	870
17/09/2015	08:23:00	N 44° 1,64359'	E 30° 44,1023'	Short term piezometer recovery YOYO2	215
17/09/2015	09:57:19	N 44° 1,59045'	E 30° 44,43833'	SMF-SDS	255
17/09/2015	10:52:09	N 44° 5,73609'	E 30° 46,66156'	Calypso CS02 lost	161
17/09/2015	12:18:41	N 44° 5,76028'	E 30° 46,74883'	SMF-SDS	160
17/09/2015	15:33:49	N 43° 57,36979'	E 30° 45,97186'	Interface corer IS01	672
17/09/2015	16:31:27	N 43° 57,35812'	E 30° 46,03649'	SMF-SDS	680
17/09/2015	16:44:10	N 43° 57,20526'	E 30° 45,26415'	Interface corer IS02 IS03	641
17/09/2015	18:50:12	N 43° 57,20643'	E 30° 45,07468'	SMF-SDS	626
17/09/2015	19:30:05	N 43° 57,83446'	E 30° 45,03117'	Transit	
17/09/2015	19:47:29	N 43° 57,99388'	E 30° 45,0404'	Penfeld CPT02	557
18/09/2015	10:29:21	N 43° 55,38616'	E 30° 45,49419'	Transit	
18/09/2015	11:35:00	N 43° 55,45508'	E 30° 45,45614'	Short term piezometer recovery YOYO3	667
18/09/2015	12:06:35	N 43° 55,44517'	E 30° 45,45881'	Transit	
18/09/2015	12:34:28	N 43° 55,21286'	E 30° 45,53005'	Heat Flux Measurements	689
18/09/2015	18:22:14	N 43° 56,60016'	E 30° 45,04909'	Transit	
18/09/2015	19:58:34	N 43° 57,78356'	E 31° 3,5149'	Penfeld CPT03	874
19/09/2015	06:58:23	N 43° 58,23824'	E 31° 0,62725'	Transit	
19/09/2015	07:19:22	N 43° 58,07894'	E 31° 2,58253'	Calypso CS01	830
19/09/2015	10:39:41	N 43° 58,0383'	E 31° 3,1141'	SMF-SDS	845
19/09/2015	12:36:29	N 43° 58,4616'	E 30° 59,62314'	Gravity core GC01	
19/09/2015	14:27:53	N 43° 58,39753'	E 30° 59,73356'	Interface corer IS04	235
19/09/2015	16:00:40	N 43° 58,3933'	E 30° 59,76977'	Short term piezometer deployment failed YOYO4	789
19/09/2015	19:58:48	N 43° 58,39042'	E 30° 59,77113'	SMF-SDS	793
19/09/2015	20:40:03	N 44° 0,57622'	E 30° 57,56488'	Penfeld CPT04	644

20/09/2015	06:33:00	N 43° 59,52541'	E 30° 57,45266'	SMF-SDS	667
20/09/2015	09:07:54	N 43° 42,45079'	E 31° 6,55812'	Calypso CS04	1622
20/09/2015	11:28:35	N 43° 42,45516'	E 31° 6,57507'	SMF-SDS	1622
20/09/2015	13:49:43	N 43° 58,38235'	E 30° 59,65031'	Interface corer IS05	808
20/09/2015	14:59:27	N 43° 58,4009'	E 30° 59,73729'	Calypso CS05	795
20/09/2015	16:51:06	N 43° 58,53962'	E 30° 59,41349'	Transit	
20/09/2015	17:31:11	N 44° 0,58893'	E 30° 57,49249'	Penfled VP01	655
21/09/2015	04:13:53	N 43° 59,23734'	E 30° 56,92135'	Transit	
21/09/2015	04:25:39	N 43° 59,47393'	E 30° 57,25021'	Calypso CS06	659
21/09/2015	06:27:22	N 43° 59,48665'	E 30° 57,30518'	SMF	647
21/09/2015	07:16:54	N 43° 55,68466'	E 30° 50,93544'	Interface corer IS06	853
21/09/2015	08:15:09	N 43° 56,02997'	E 30° 51,1438'	Transit	
21/09/2015	08:26:11	N 43° 56,35545'	E 30° 51,03633'	Interface corer IS07	731
21/09/2015	10:05:44	N 43° 56,69928'	E 30° 50,0915'	SMF	770
21/09/2015	11:17:16	N 43° 56,02892'	E 30° 51,14797'	Gravity Core GC02	755
21/09/2015	12:42:54	N 43° 56,02981'	E 30° 50,66759'	Interface corer IS08	
21/09/2015	13:23:29	N 43° 56,02443'	E 30° 50,66182'	Transit	
21/09/2015	14:36:35	N 43° 58,4408'	E 30° 59,76166'	Short term piezometer deployment YOYO5	801
21/09/2015	19:07:51	N 43° 58,71987'	E 30° 59,55808'	Transit	
21/09/2015	19:47:54	N 43° 56,33537'	E 30° 51,79231'	Penfeld CPT05	794
22/09/2015	06:31:24	N 43° 55,91106'	E 30° 50,11609'	Transit	
22/09/2015	07:14:55	N 43° 58,19356'	E 30° 49,55108'	CTD no acquisition	646
22/09/2015	08:39:19	N 43° 58,17144'	E 30° 49,3438'	SMF	667
22/09/2015	09:12:34	N 43° 56,04948'	E 30° 50,58125'	Gravity Core GC03	820
22/09/2015	10:54:20	N 43° 56,12908'	E 30° 50,64361'	Transit	
22/09/2015	11:21:28	N 43° 58,18597'	E 30° 49,33619'	CTD no acquisition	660
22/09/2015	13:57:30	N 43° 58,1919'	E 30° 49,33338'	Transit	
22/09/2015	14:30:13	N 43° 56,29983'	E 30° 51,79885'	Penfled VP02	797
23/09/2015	02:34:29	N 43° 56,04128'	E 30° 50,64299'	Transit	
23/09/2015	02:40:06	N 43° 56,04137'	E 30° 50,66715'	Calypso CS07	
23/09/2015	04:17:42	N 43° 56,12059'	E 30° 50,71838'	SMF	809
23/09/2015	05:20:41	N 43° 56,4454'	E 30° 51,66898'	Heat Flux Measurement	787
23/09/2015	11:13:12	N 43° 55,92184'	E 30° 50,20848'	Transit	
23/09/2015	11:38:43	N 43° 58,22253'	E 30° 49,61087'	CTD	638
23/09/2015	16:32:00	N 43° 58,06393'	E 30° 49,49077'	SMF	661
23/09/2015	16:49:57	N 43° 56,08965'	E 30° 50,54857'	CALYSPO CS08	828
23/09/2015	19:12:33	N 43° 56,02994'	E 30° 50,69923'	Short term piezometer deployment YOYO6	835
23/09/2015	21:51:48	N 43° 55,94114'	E 30° 50,88261'	Transit	
23/09/2015	22:36:39	N 43° 55,25574'	E 30° 45,54519'	Penfeld CPT06	695
24/09/2015	10:27:31	N 43° 57,76795'	E 30° 45,57154'	SMF	638
24/09/2015	11:28:56	N 44° 5,19308'	E 30° 47,97321'	Interface Corer IS09	242
24/09/2015	11:49:57	N 44° 5,19319'	E 30° 47,9747'	SMF	242
24/09/2015	12:23:20	N 44° 5,756'	E 30° 46,60536'	Interface Corer IS10	161
24/09/2015	12:53:41	N 44° 5,74433'	E 30° 46,61737'	Calypso CS09	161
24/09/2015	13:56:36	N 44° 5,58062'	E 30° 46,57876'	SMF	164
24/09/2015	15:19:23	N 43° 55,55311'	E 30° 45,29087'	Calypso CS10	651
24/09/2015	18:20:10	N 43° 55,43657'	E 30° 45,37949'	Transit	
24/09/2015	18:51:15	N 43° 55,19852'	E 30° 45,52823'	Penfeld VP03	691
25/09/2015	09:31:11	N 43° 56.36396'	E 30° 44.78437'	SMF	632
25/09/2015	10:39:24	N 43° 49.89188'	E 30° 32.70105'	Calypso CS11	738
25/09/2015	14:17:07	N 43° 50.30724'	E 30° 33.52376'	ANITRA	812

25/09/2015	15:32:19	N 43° 50.74469'	E 30° 32.75028'	Transit	
25/09/2015	15:59:32	N 43° 50.15834'	E 30° 34.26911'	Multitube MTB01	
25/09/2015	18:03:21	N 43° 50.13879'	E 30° 34.30496'	Transit	
25/09/2015	19:26:30	N 43° 56.77136'	E 30° 50.9478'	Penfeld CPT07	708
26/09/2015	05:11:03	N 43° 54.66806'	E 30° 51.37823'	SMF	961
26/09/2015	05:38:19	N 43° 55.56141'	E 30° 50.63252'	Piezometer Recovery YOYO6	882
26/09/2015	06:39:00	N 43° 56.06296'	E 30° 50.60505'	Transit	
26/09/2015	07:14:24	N 43° 58.00016'	E 30° 45.01828'	Calypso CS12	552
26/09/2015	09:39:57	N 43° 57.99386'	E 30° 45.00646'	SMF	549
26/09/2015	10:50:27	N 43° 58.29176'	E 30° 59.28825'	Piezometer Recovery YOYO5	822
26/09/2015	12:27:26	N 43° 58.92622'	E 30° 58.29327'	Calypso CS13	750
26/09/2015	14:55:05	N 43° 59.29391'	E 30° 57.21138'	SMF	665
26/09/2015	15:15:26	N 44° 0.18028'	E 30° 56.38729'	Penfeld CPT08	621
27/09/2015	03:17:50	N 43° 59.5924'	E 30° 56.976'	Transit	643
27/09/2015	03:48:23	N 43° 57.15253'	E 30° 52.35493'	SMF	758
27/09/2015	04:00:01	N 43° 56.2865'	E 30° 51.053'	Calypso CS14	751
27/09/2015	05:50:41	N 43° 56.36734'	E 30° 51.04097'	Transit	
27/09/2015	06:08:23	N 43° 56.03999'	E 30° 50.65367'	Interface corer IS11	
27/09/2015	07:12:59	N 43° 55.82891'	E 30° 50.48666'	SMF	872
27/09/2015	07:24:19	N 43° 55.29377'	E 30° 50.85595'	SMF	894
27/09/2015	09:52:08	N 43° 56.02189'	E 30° 50.68148'	Long term Piezometer deployment PZ1	824
27/09/2015	11:38:05	N 43° 56.04461'	E 30° 50.7306'	SMF	822
27/09/2015	12:02:54	N 43° 56.60967'	E 30° 47.09814'	Heat flux measurements	776,4
27/09/2015	15:56:07	N 43° 57.22117'	E 30° 45.96387'	SMF	683
27/09/2015	16:38:07	N 43° 55.5474'	E 30° 45.32507'	Calypso CS15	655,2
27/09/2015	18:32:46	N 43° 55.53023'	E 30° 45.29911'	Transit	
27/09/2015	19:15:46	N 43° 56.81115'	E 30° 50.91365'	Penfeld VP04	705
28/09/2015	03:43:15	N 43° 56.11345'	E 30° 51.26019'	SMF	771
28/09/2015	04:38:22	N 43° 57.34958'	E 30° 46.01613'	Calypso CS16	690
28/09/2015	06:46:35	N 43° 57.38441'	E 30° 46.00922'	SMF	681
28/09/2015	07:26:01	N 43° 55.47452'	E 30° 45.44252'	STATION76	660
28/09/2015	07:31:40	N 43° 55.46046'	E 30° 45.44164'	Long term Piezometer deployment PZ2	664
28/09/2015	09:12:06	N 43° 55.47469'	E 30° 45.44626'	SMF	666
28/09/2015	10:00:49	N 43° 55.72941'	E 30° 50.45882'	CTD	884
28/09/2015	15:27:12	N 43° 55.89007'	E 30° 50.16725'	Heat flux measurements	882
28/09/2015	20:01:30	N 44° 0.50821'	E 30° 57.52823'	Transit	
28/09/2015	20:27:21	N 44° 0.5852'	E 30° 57.54957'	Calypso CS17	652,2
28/09/2015	23:38:18	N 44° 0.60787'	E 30° 57.52934'	SMF	651
29/09/2015	00:43:56	N 43° 55.26466'	E 30° 45.32696'	Interface corer IS12	664
29/09/2015	01:49:12	N 43° 55.58431'	E 30° 45.28571'	Transit	
29/09/2015	01:57:07	N 43° 55.78262'	E 30° 45.29819'	Calypso CS18	641
29/09/2015	05:58:00	N 43° 56.0371'	E 30° 36.26703'	Transit	

Table 4: Course of the Leg 2.

V. GEOPHYSICAL DATA ACQUISITION

V.1. Bathymetry and Seafloor reflectivity

The R/V Pourquoi pas ? is fitted with two multibeam echosounders :

- the Reson seabat 7111, for shallow water, mounted on the hull,
- the Reson seabat 7150, for mid and deep water, mounted on a gondola below the hull.

The upper shelf was surveyed by both sounders, while the lower part was only surveyed by the seabat 7150, as illustrated by the map presented in Figure 2. This figure presents the ship tracks made for bathymetry acquisition.

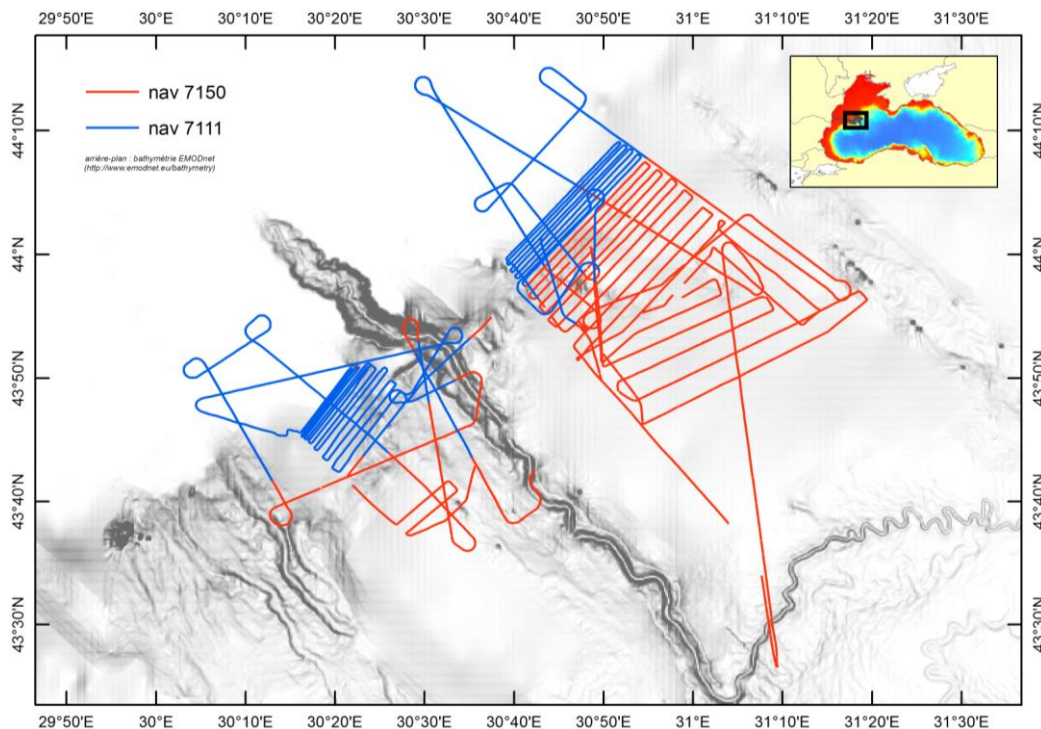


Figure 2: survey tracks for bathymetry acquisition.

Data were processed using Caribes and Sonarscope softwares, and following a two-step process:

- automated filtering based on soundings quality factor (QF) and morphologic continuity,
- manual inspection and editing.

The QDTMF is an estimate of the seafloor bottom detector accuracy. It is computed from:

- signal envelope width, for amplitude detections (near nadir beams),
- phase signal to noise ratio, for interferometric detections (grazing beams).

Figure 3 shows a DTM from the seabat 7111 and 7150 data acquired during the GHASS cruise.

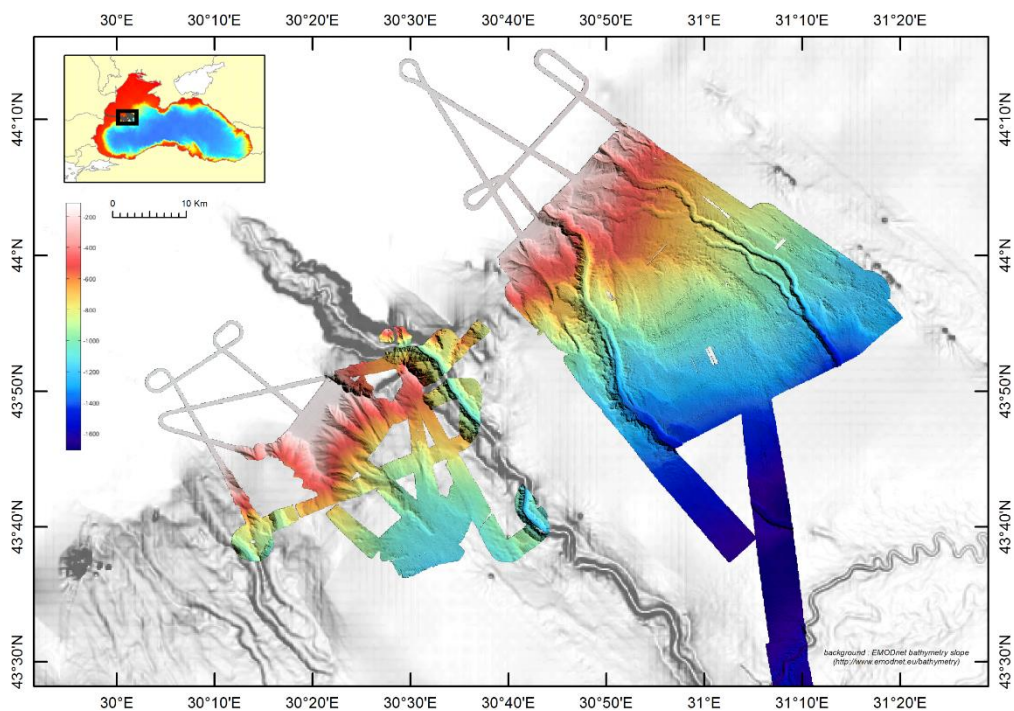


Figure 3: shaded DTM made of seabat 7111 and 7150 data, 15m grid.

Reflectivity data were processed in order to cope with any artefact due to the echosounder and seafloor backscatter, to deliver the smoothest possible image. This means that data were compensated from :

- echosounder beam pattern,
- echosounder gain,
- simulated seafloor angular backscatter pattern.

Only signal samples corresponding to previously validated soundings were considered. Figure 4 presents the reflectivity obtained from seabat 7150 data.

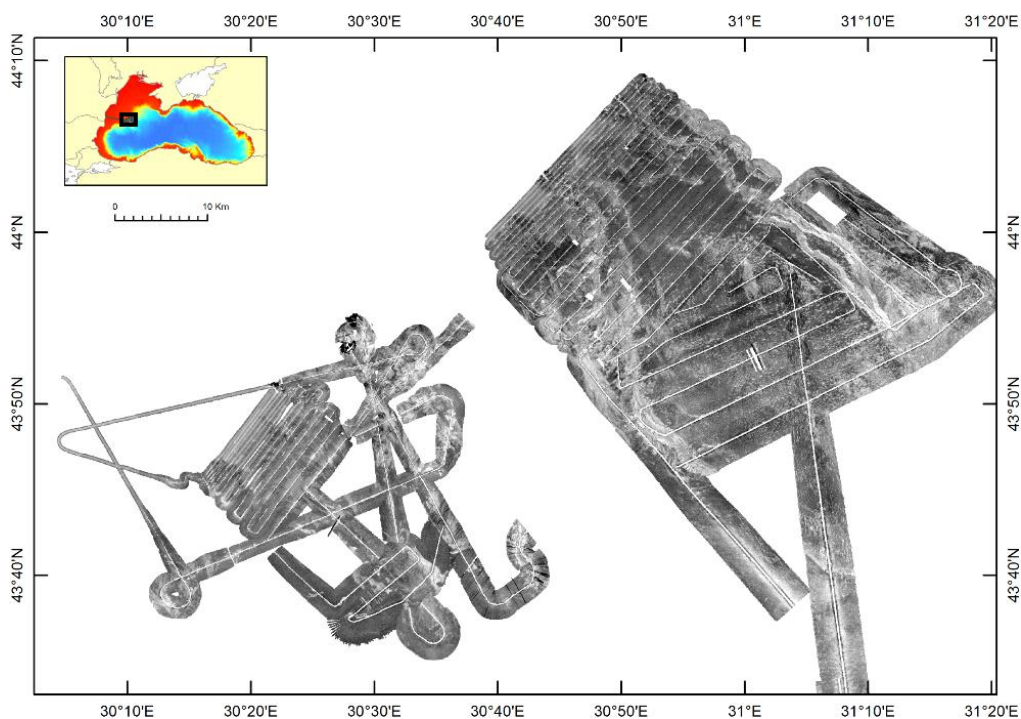


Figure 4: Reflectivity mosaic of seabat 7150 data, 15m grid.

V.2. Sub-bottom Profiler

The hull-mounted sub-bottom profiler of the Pourquoi Pas? operates at the frequency range (1800–5000 Hz), giving a vertical resolution close to 20 cm. The lateral resolution is constrained by the water depth below the instrument. The water depth of 800 m restricted the lateral resolution of the hull-mounted SBP to 15 m.

The SBP data were acquired by using the SUBOP software (acquisition parameters given in table 5). These data were acquired during the bathymetry acquisition. The quality control of the SBP data was made by QC Subop developed by Ifremer. Figure 5 presents some SBP profiles acquired during the GHASS cruise.

Configuration GHASS	2	3	7	8
configuration	50-500 m	> 500 m	> 500 m	50-500 m
% emission	30	100	100	50
sweep duration [ms]	50	80		50
record length [ms]	250	250	350	250
configuration	simple	intricate		simple
shot interval [ms]	800	800	800	800
Delay [ms]	60	60	60	60
time window before seafloor [ms]	50	50	50	50
Time interval between two simple shot [ms]	100	100	100	100
Time interval between two intricate shot [ms]	100	100	100	100
Max Number of intricate shots	6	6	6	6

Table 5: Acquisition parameters of the SBP.

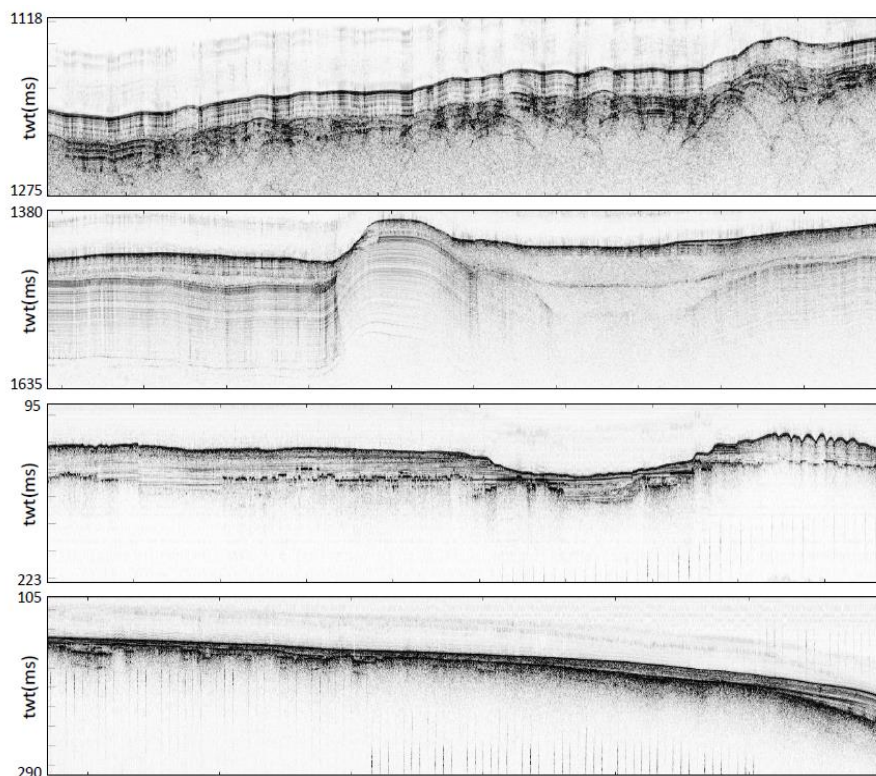


Figure 5: SBP profiles acquired during the GHASS cruise.

V.3 Water column acoustic acquisition

Acquisition

Water column acoustic data were recorded continuously during the first leg, except during the dives of the seismic deep-towed system, following two configurations:

- SMF7150 for deep water depth,
- SMF7111 for shallow water depth.

A dedicated water column acoustic acquisition was performed on bubble seepage sites on the 14th September 2015. During the second leg, dedicated water column acoustic acquisitions were performed on bubble seepage sites and coring sites. Water column acoustic data were also acquired during bathymetry acquisition. A full description of multibeam echosounder's characteristics can be found in Table 6.

Parameters	7150-LF	7150-HF	7111
Sonar Operating Frequency	Centered on 12kHz	Centered on 24kHz	100kHz
Across-Track Beam Width at Nadir Beam*	1°	0.5°	1.8°
Along-Track Beam Width	1°	0.5°	1.5°, 3.0°, 4.5°, or 6.0° (operator selected)
Number of Across-Track Beams	256 Equi-angle or 880 Equi-distant.		101 or 201 equi-angle, 301 Equi-distant
Swath Coverage	Up to 150° with maximum swath width** of approximately 5.5 times the water depth.		
Depth (typical)	200 - 7000 meters	200 - 4000 meters	5 - 1000 meters
Ping Rate	Up to 15 pings per second		Up to 20 pings per second
Pulse Length (CW)	0.5 - 20 msec (mode and range dependent)		170µsec to 3msec
Pulse length (FM)	200msec		N/A
Main sample rate	6022 Hz		
Bottom Detection Resolution	200-400m: 12 cm 600-800m: 25 cm 1200-1600m: 50 cm 2400-4800m: 1m 6400+ m: 2m	200-400m: 12 cm 400-600m: 25 cm 800-1200m: 50 cm 1600-2400 m: 1m 3200+ m: 2m	12 cm

Table 6: Descriptions of multibeam echosounders.

Onboard Processing

The layout of processed acoustic data tracks is displayed in Figure 6. Acoustic data were processed with sonarscope software (Fig. 7) and visualized with Globe software (Fig. 8). The data processing was made on average amplitude data but we also processed a few profiles with amplitude and phase data. The methodology used for picking bubble echos can be found in the technical report dedicated to water column acoustics.

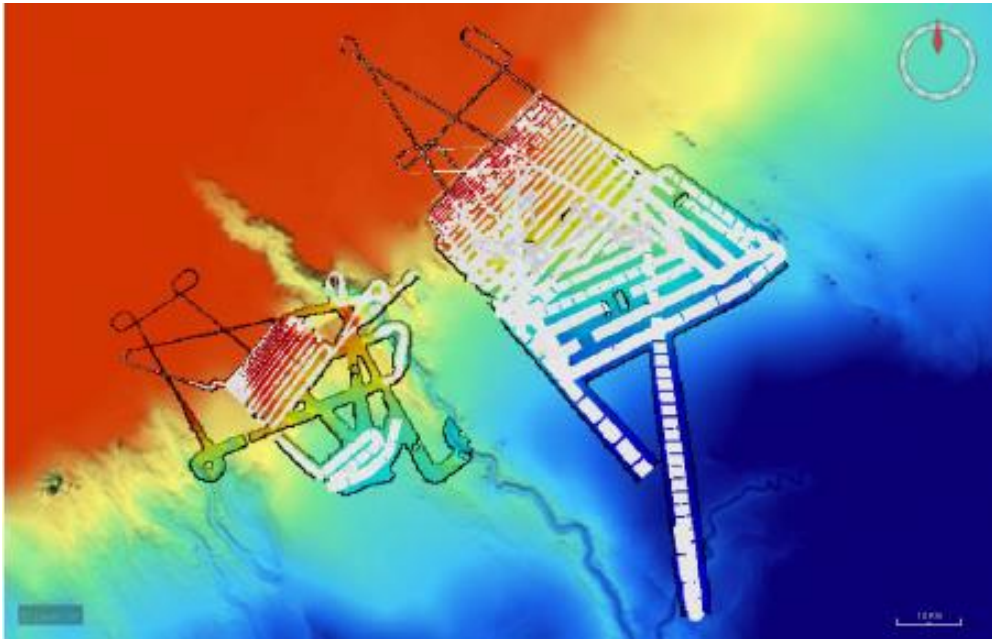


Figure 6: Map of the layout of acoustic data tracks.

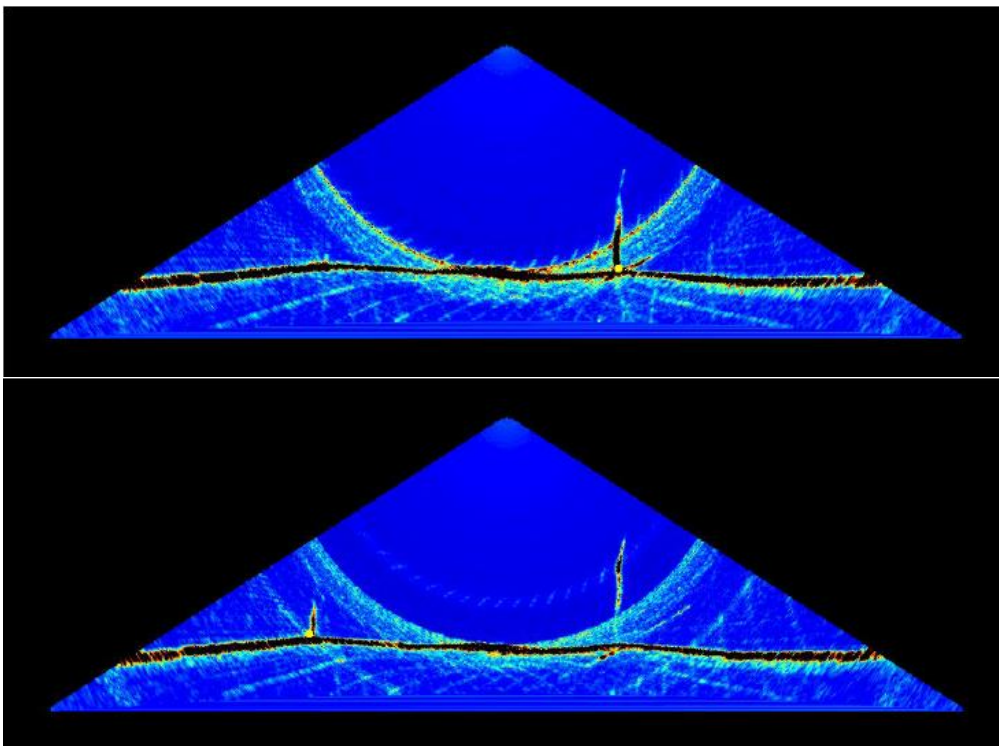


Figure 7: Examples of echogram presenting bubble seepages.

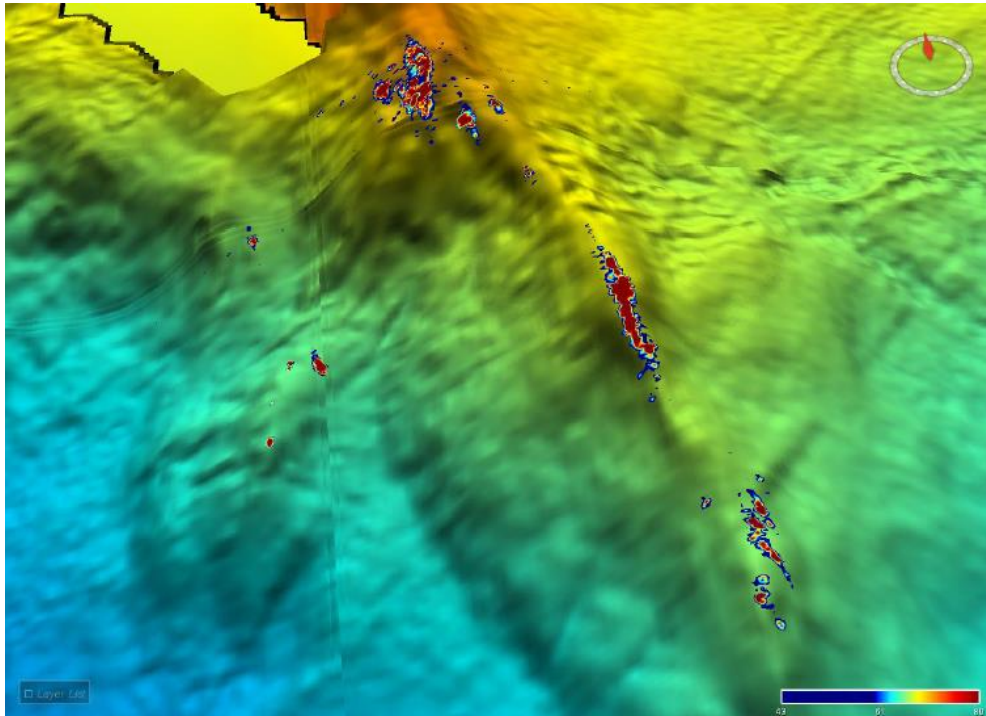


Figure 8: Visualisation of seepage sites with Globe.

V.4. High Resolution Seismic Acquisition

HR seismic data were acquired by the new acquisition system SEAL428 associated with the solid streamer (SENTINEL® Solid Acquisition Sections RD). The solid streamer has 96 traces with a 6.25 m spacing between traces. The depth of the source and the streamer were set at 2 m except for the two last profiles. Mini-GI guns were used as seismic sources (24/24 and 13/13). Most of the acquisition was done with a single 24/24 Mini-GI gun towed at 2 m depth. The mean signature of the 24/24 Mini-GI gun has a frequency bandwidth [45-190] Hz with a central frequency at 115 Hz (Fig. 9). 21 profiles were acquired in two sequences. Tables 7 and 8 describe the acquisition parameters used for each profile.

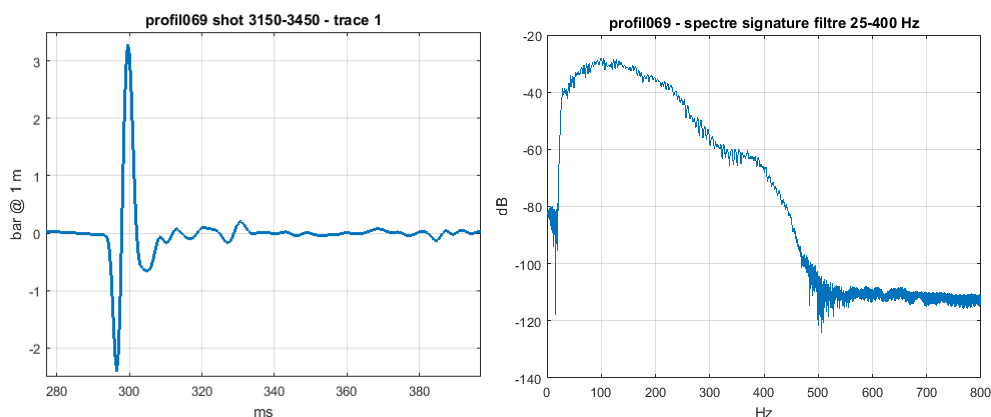


Figure 9: Mean Signature of the 24/24 ci Gun (pressure 140 bar, gun and streamer depth 2 m) computed from the seafloor reflection and its related multiple. Amplitude level: -2.4 / +3.3 bar à 1 m, filter 25-400 Hz ; Bandwidth -6 dB [45-190] Hz, Central frequency 115 Hz.

A quality control was made by using Ifremer softwares SolidCheck and SolidQC. The mean level of noise was 1 μ bar for the whole cruise (Fig. 10). With identical sea conditions, the mean

level of noise recorded by the former system was 2.5 μ bar which highlights the better performance of the new streamer compared to the previous one.

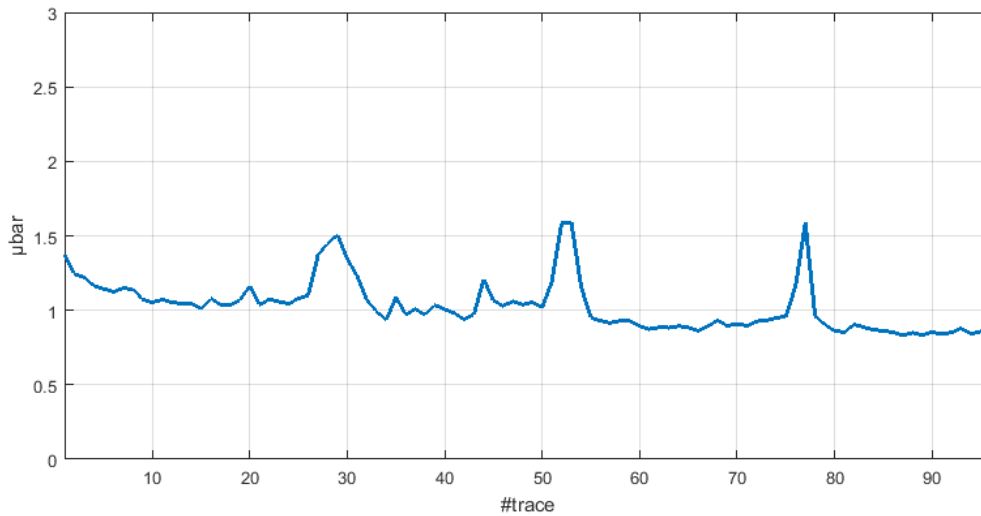


Figure 10: Mean level of noise per traces for the whole survey (frequency filter : 35-375 Hz).

Profile	Area	Sonde.[m]	Shots	Date (end of profile)	Source	Mean heading	Streamer depth
GAS030.1	N	1660-828	1-4949	03/09/2015	2x24/24 (1+2) 2x24/24 (1+3)	352°	2 m
GAS031.1	N	989-108	1-7052	04/09/2015	1x24/24 (2)	302°	2 m
GAS033.1	N	108-470	1-3925	04/09/2015	1x24/24 (2)	148°	2 m
GAS033.1	N	470-981	3926-5296	04/09/2015	1x24/24 (2)	131°	2 m
GAS034.1	N	954-749	1-1600	04/09/2015	1x24/24 (2)	69°	2 m
GAS034.1	N	708-862	1601-3870	04/09/2015	1x24/24 (2)	50°	2 m
GAS035.1	N	830-1148	1-1884	04/09/2015	1x24/24 (3)	127°	2 m
GAS036.1	N	1124-114	1-6648	05/09/2015	1x24/24 (3)	306°	2 m
GAS037.1	N	125-139	1-2685	05/09/2015	1x24/24 (3)	223°	2 m
GAS038.1	N	134-775	1-2047	05/09/2015	1x24/24 (2)	142°	2 m
GAS039.1	N	570-691	1-845	05/09/2015	1x24/24 (2)	213°	2 m
GAS040.1	N	262-467	1-1961	05/09/2015	1x13/13 (1)	44°	2 m
GAS041.1	N	324-976	1-1952	05/09/2015	1x13/13 (1)	179°	2 m

Table 7: Acquisition parameters for the profiles acquired in the North area.

Profile	Area	Sonde.[m]	Shots	Date (end of profile)	Source	Mean heading	Streamer depth
GAS062.1	Sud	101-962	1-5069	09/09/2015	1x24/24 (1)	77°	2 m
GAS063.1	Sud	950-303	1-1292	09/09/2015	1x24/24 (2)	211°	2 m
GAS064.1	Sud	494-1014	1-1152	09/09/2015	1x24/24 (2)	63°	2 m
GAS066.1	Sud	562-901	1-3801	09/09/2015	1x24/24 (2)	247°	2 m
GAS067.2	Sud	747-85	1-3104	09/09/2015	1x24/24 (2)	330°	2 m
GAS068.1	Sud	72-120	1-1567	09/09/2015	1x24/24 (2)	57°	2 m
GAS069.1	Sud	92-1135	1-6353	10/09/2015	1x24/24 (2)	130°	2 m
GAS070.1	Sud	1135-304	1-3799	10/09/2015	1x24/24 (2)	350°	2,5 m
GAS071.1	Sud	329-1019	1-3988	10/09/2015	1x24/24 (2)	151°	3 m
GAS072.1	Nord	1173-463	1-2475	10/09/2015	1x24/24 (2)	336°	3 m

Table 8: Acquisition parameters for the profiles acquired in the South area.

Figure 11 presents the layout of the HR seismic survey and Figures 12 and 13 present example of HR profiles on a BSR zone and on the shelf characterized by the presence of free gas.

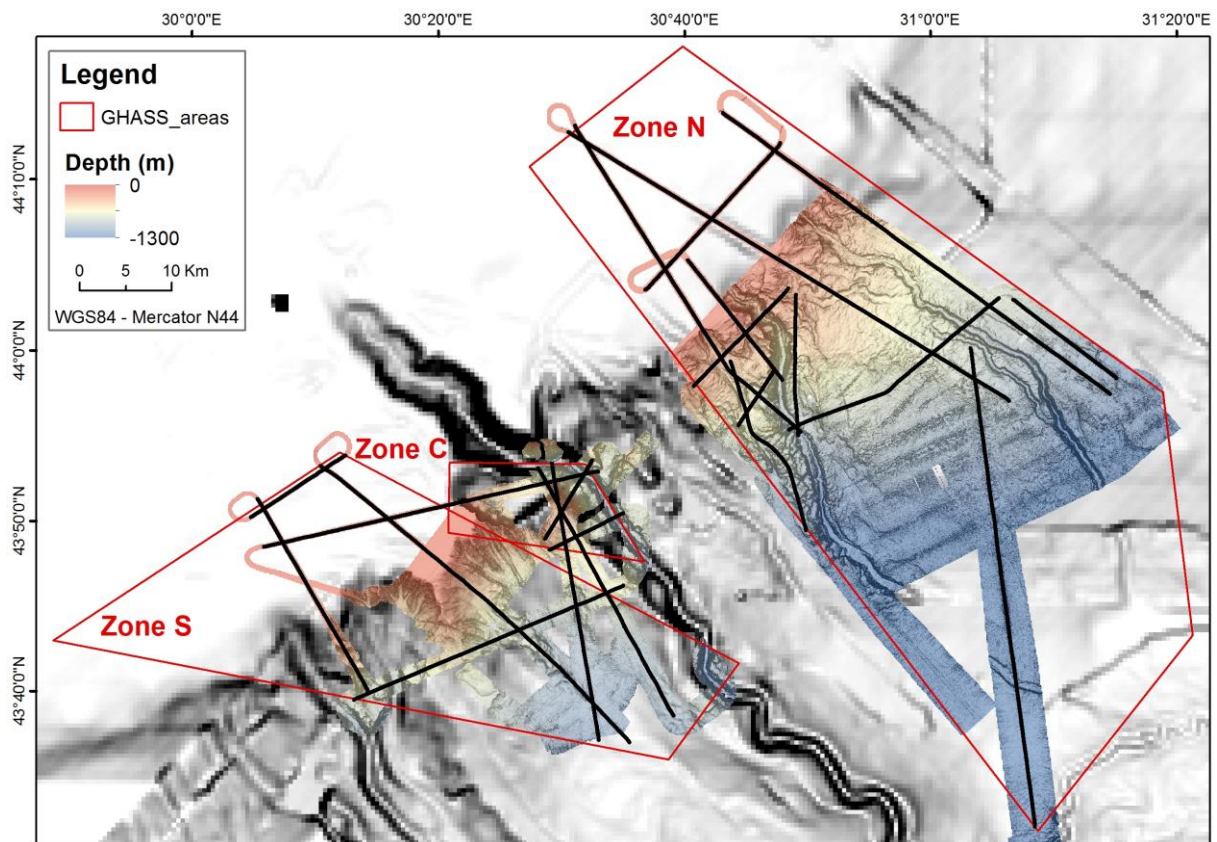


Figure 11: Location map of the HR seismic data.

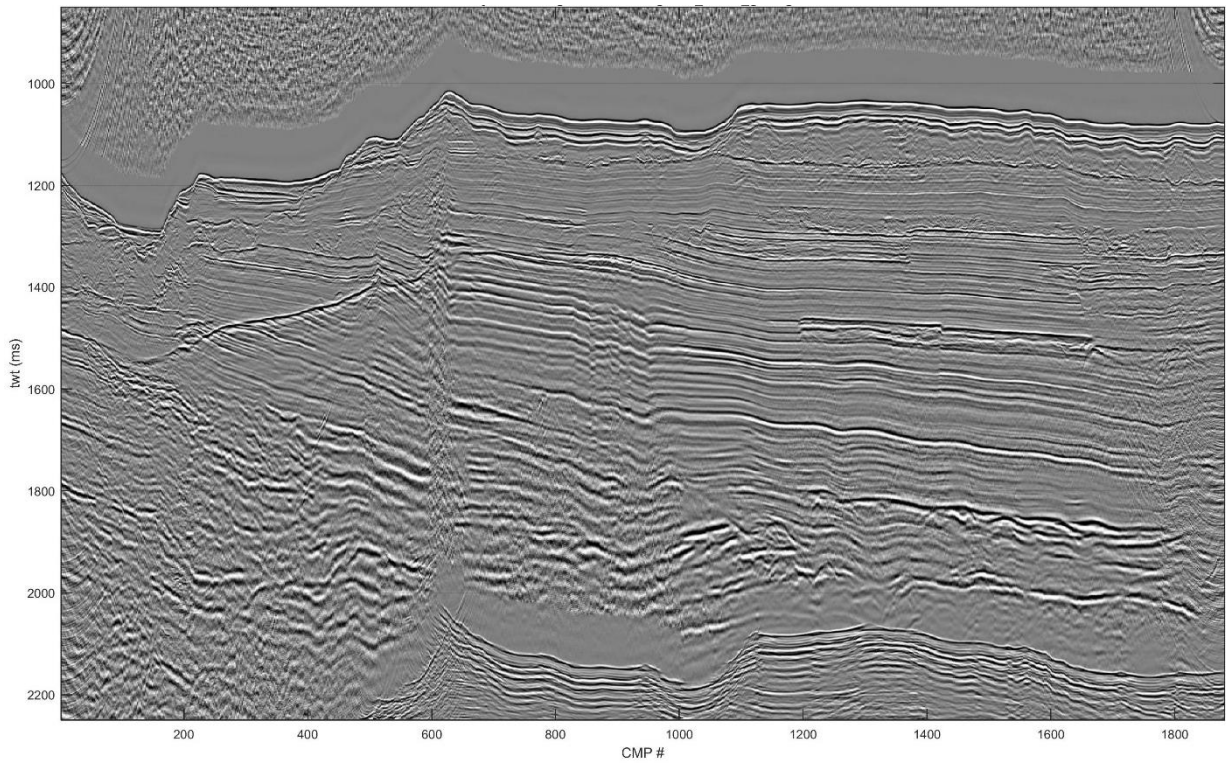


Figure 12: Part of the profile GAS034 (stack and migration with constant velocity, AGC with a 100ms window).

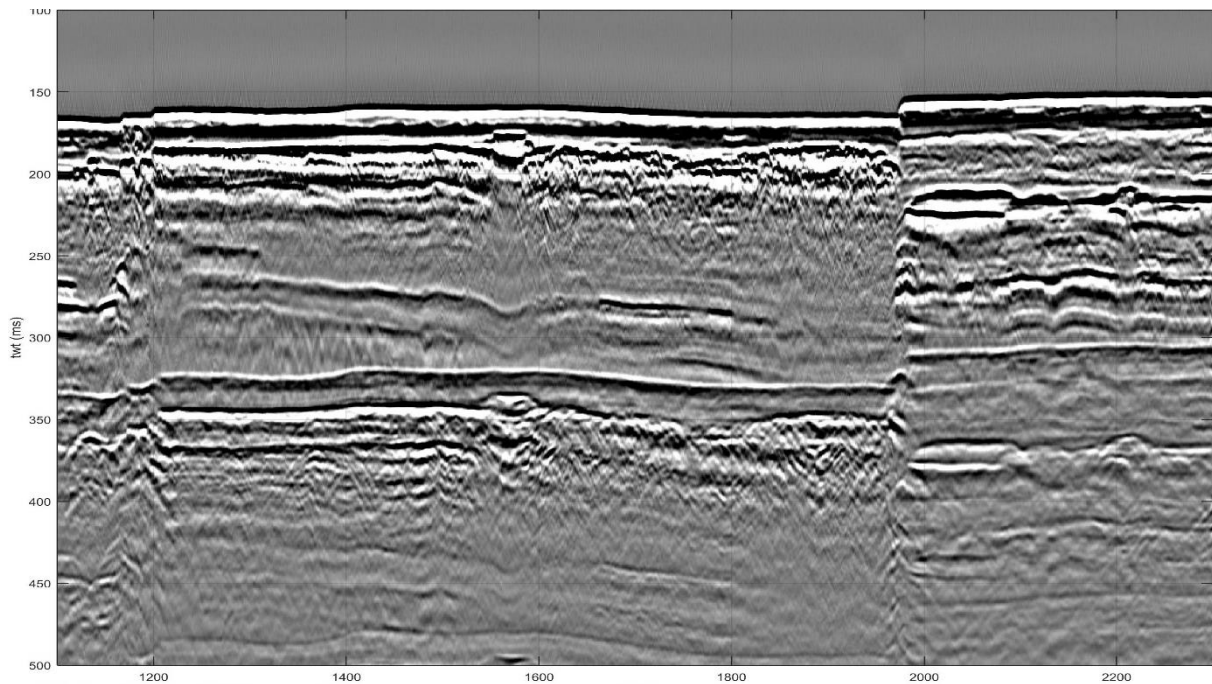


Figure 13: Part of the profile GAS031 acquired on the shelf (stack and migration with a velocity gradient of 250 m/s).

V.4. SYSIF deep-towed seismic acquisition

The SYSIF deep-towed seismic system has been recently developed by Ifremer and is far more effective in the quality of its imaging and the degree of sub-seabed penetration than earlier systems of a similar type. The system is usually towed at 2 knots about 50-100 m above

the seabed. Towing both the source and streamer close to the seabed confers the advantages of a very small first Fresnel zone (compared with a surface source and streamer), significantly improving horizontal resolution and reducing interference from reflections and diffractions out of the plane of the seismic section. Also, signal-to noise is much improved, because of the quieter environment and because the source and receiver are closer to the target reflectors. The Janus-Helmholtz 220-1050Hz was used for the whole survey. A chirp is emitted with a linear frequency modulation and a duration of 100 ms. A prototype of a multichannel streamer (50 hydrophones with 2 m spacing) was used to improve the seismic imaging and to perform a high resolution velocity analysis. Two profiles were focused on the velocity analysis by setting the altitude of the device at 50 m in order to increase the incidence angle range. During the cruise, three dives were made: two in the North area and one in the South Area (Fig. 14). Tables 9 to 11 described the acquisition parameters of the 30 SYSIF profiles and Figure 15 shows an example of SYSIF profiles acquired during the first dive.

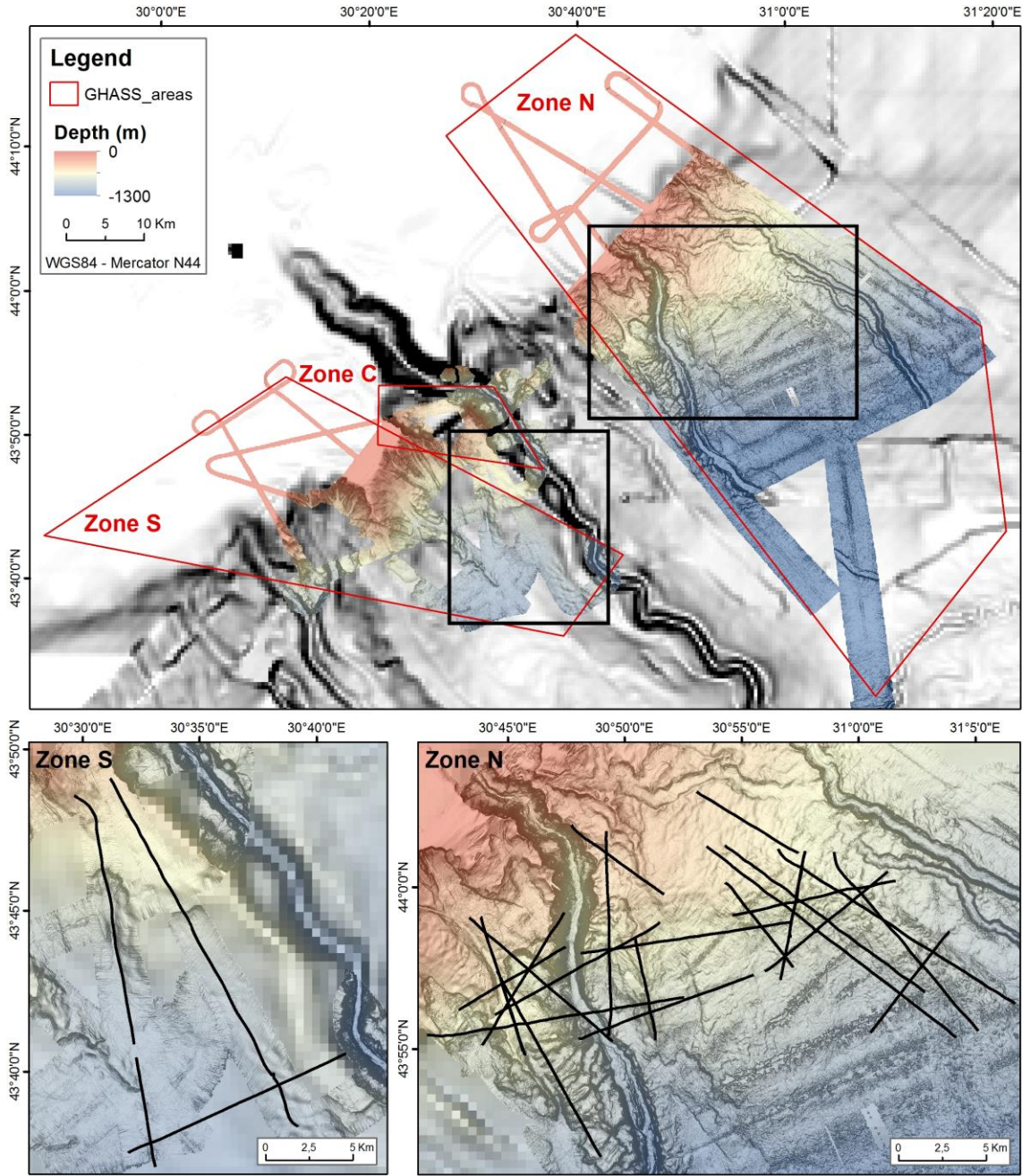


Figure 14: Location map of the Sysif seismic data.

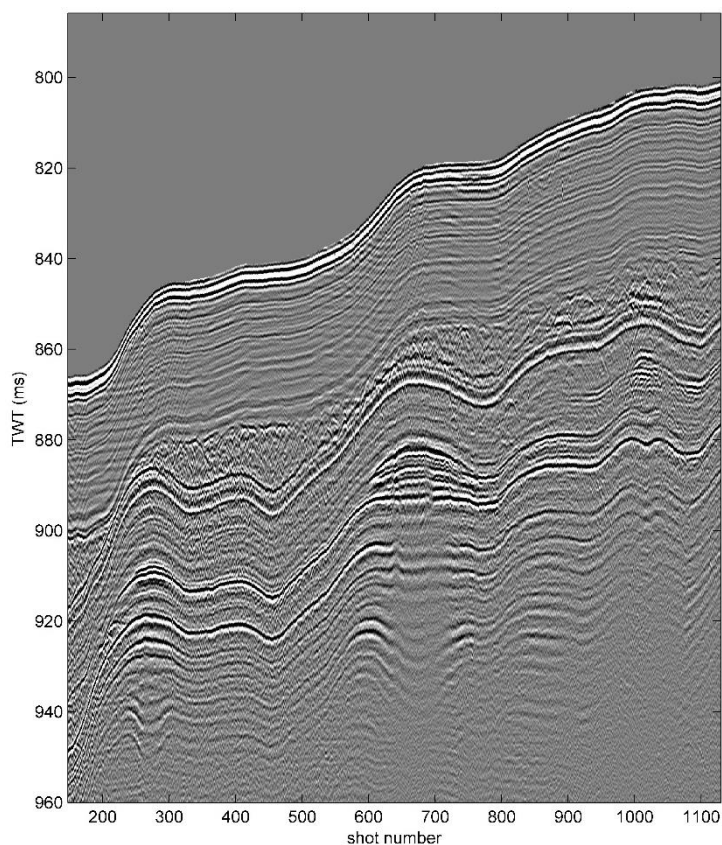


Figure 15: Example of SYSIF profiles acquired during the first dive.

Profile	Area	Shots	Date (end of profile)	Altitude	Shot Interval	Length
PL01PR01	N	3982	05/09/2015	100 m	2.2 s	8.9 km
PL01PR02	N	3517	05/09/2015	100 m	2.2 s	8.3 km
PL01PR02B	N	1667	06/09/2015	50 m	2.2 s	3.75 km
PL01PR03	N	4244	06/09/2015	100 m	2.6 s	10.8 km
PL01PR04	N	3890	06/09/2015	100 m	2.6 s	11.6 km
PL01PR05	N	2673	06/09/2015	100 m	2.2 s	6.5 km
PL01PR06	N	4015	06/09/2015	100 m	2.6 s	10.7 km
PL01PR07	N	4000	06/09/2015	100 m	2.6 s	10.7 km
PL01PR08	N	3570	06/09/2015	100 m	2.4 s	9.1 km
PL01PR09	N	3728	07/09/2015	100 m	2.4 s	9.5 km
PL01PR10	N	2493	07/09/2015	100 m	2.4 s	6.2 km
PL01PR11	N	2927	07/09/2015	100 m	2.4 s	7.4 km
PL01PR12	N	4585	07/09/2015	100 m	2.4 s	13.2 km
PL01PR13	N	3688	07/09/2015	100 m	2.6 s	
PL01PR14	N	2748	07/09/2015	100 m	2.3 s	6.75 km

Table 9: Acquisition parameters of SYSIF profiles acquired during the first dive

Profile	Area	Shots	Date (end of profile)	Altitude	Shot Interval	Length
PL02PR01-01	N	4873	10/09/2015	100 m	2.9 s	14.7 km
PL02PR01-02	N	2147	11/09/2015	100 m	2.9 s	6.4 km
PL02PR02	N	4199	11/09/2015	100 m	3.0 s	13.7 km
PL02PR03	N	7754	11/09/2015	100 m	2.7 s	22.6 km

Table 10: Acquisition parameters of SYSIF profiles acquired during the second dive

Profile	Area	Shots	Date (end of profile)	Altitude	Shot Interval	Length
PL01PR01	N	4420	12/09/2015	100 m	2.6 s	12.1 km
PL01PR02	N	2692	1209/2015	100 m	2.4 s	7.1 km
PL01PR03	N	5471	12/09/2015	50 m	2.6 s	14.9 km
PL01PR04	N	2338	1309/2015	100 m	2.4 s	6.1 km
PL01PR05	N	4455	13/09/2015	100 m	2.4 s	12.2 km
PL01PR06	N	1869	13/09/2015	100 m	2.4 s	5.1 km
PL01PR07	N	5331	13/09/2015	100 m	2.9 s	16.1 km
PL01PR08	N	5252	13/09/2015	100 m	2.9 s	17.9 km
PL01PR09	N	5519	13/09/2015	100 m	2.5 s	14.1 km
PL01PR10	N	2458	1409/2015	100 m	2.9 s	7.31 km
PL01PR11	N		14/09/2015	100 m		

Table 11: Acquisition parameters of SYSIF profiles acquired during the third dive.

VI. *IN SITU* DATA ACQUISITION

VI.1. *In Situ* geotechnical and acoustic soundings (Penfeld penetrometer)

Details of the Penfeld penetrometer

The Penfeld penetrometer is a seabed rig developed by IFREMER to ensure piezocone penetration at a constant rate of 2 cm/s down to 30 m below seabed (Sultan et al., 2007, Figure 16). Piezocones are commonly used in geotechnical practice to measure tip resistance (q_c), sleeve friction (f_s) and induced pore pressures (Δu_2) (Figure 16). The measured pore pressures were used to derive corrected tip resistances (q_t). Piezocone sounding is recognised as an efficient method to obtain the geotechnical stratigraphy, lithology, shear strength and other engineering parameters. Sultan et al., (2007, 2010) have shown that piezocone sounding is an effective means of identifying gas hydrates, based on notable increases in q_t and f_s above values commonly indicative for the presence of sand.

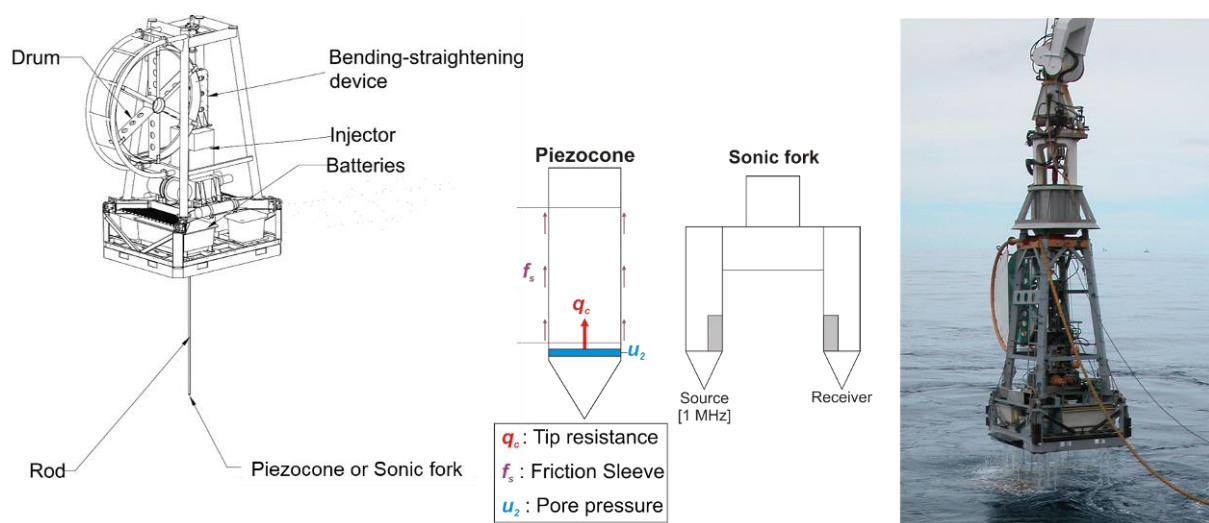


Figure 26: Illustration of the Penfeld penetrometer and of the piezocone and sonic fork that it can alternatively push down to 30 m below seabed.

By replacing the piezocone by an acoustic fork, the Penfeld penetrometer alternatively allows to acquire continuous profiles of compressional wave velocity (V_p) with an input signal frequency of 1 MHz. The distance between the source and receiver is 0.07m. The maximum value the system can measure is 2500 m/s. The V_p value recorded by the system corresponds to the average calculated over 1000 samples in half a second while the fork is pushed at a constant rate of 2 cm/s. *In situ* V_p measurement thus achieved have been shown by Sultan et al., (2007) to be instrumental for characterizing the presence of free gas or gas hydrates in sediments.

Summary of the Penfeld operations

A total number of 61 *in situ* soundings were completed with the Penfeld penetrometer and their locations are shown in Figure 17. The total length of sediment thus investigated is 1515.74 m. 46 soundings were carried out during 8 dives using piezocones (Table 12), to perform cone penetration tests with pore pressure measurements (CPTu). Additionally, 15 acoustic soundings were carried out during 4 dives using the sonic fork. 36 soundings, that is 59% of the total number, could have been completed down to the maximum penetration depth of 30m. 12 soundings were stopped before this depth as the maximum load the penetrometer could apply was reached (Applied load refusal in table 12). In these cases, one may infer that the medium was characterized by high friction. Additionally, there have been 2 cases where the soundings automatically stopped as the tip resistance exceeded the maximum value the

sensor could measure (GAS-CPTu05-S03 and GAS-CPTu07-S05, tip resistance refusal in table 12). In two other cases the soundings were automatically stopped as pore pressure rose beyond the measurement range of the differential pressure sensor (Pressure refusal in table).

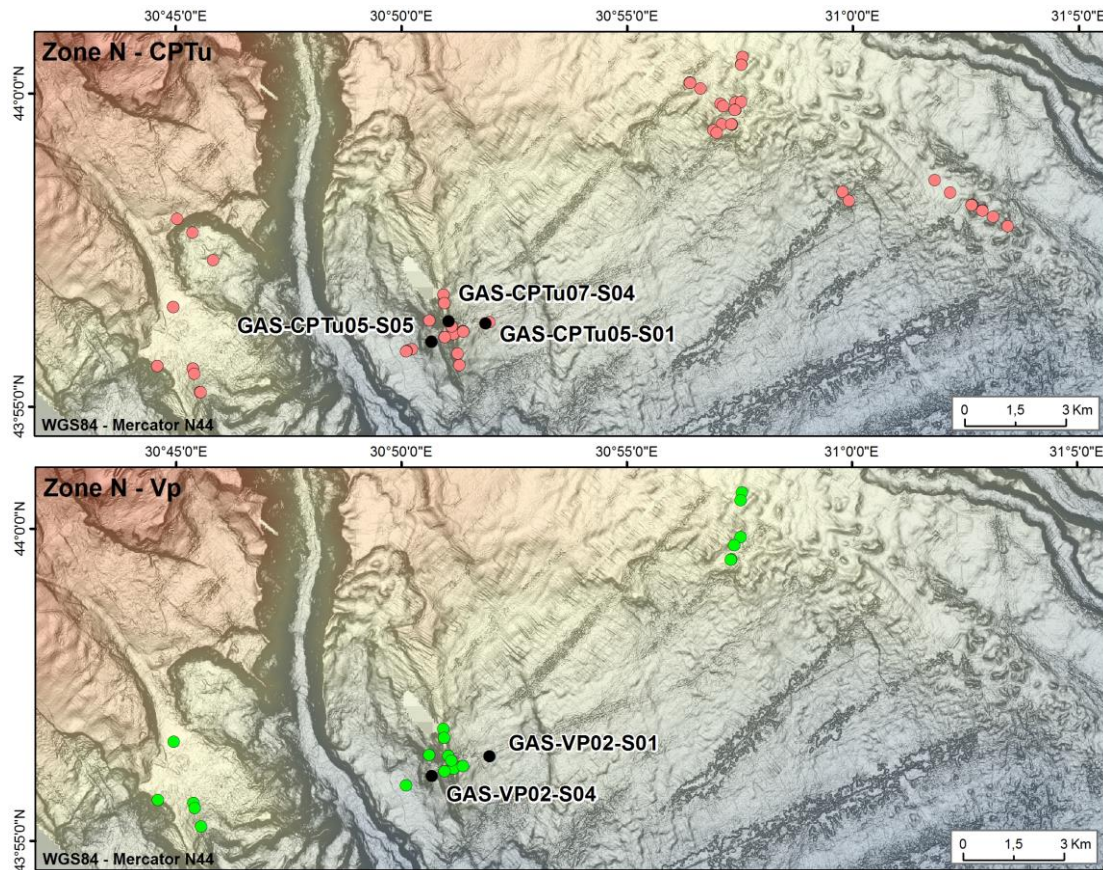


Figure 17: Bathymetric map showing the location of piezocone and acoustic sounding completed with the Penfeld penetrometer. The labels shown are only those of the soundings presented in this report.

Seventeen soundings were otherwise automatically stopped as the Penfeld penetrometer exceeded the maximum inclination of 8° it is rated for (Inclination refusal in table 12). This issue has been ascribed to the softness of the seabed sediments in which the Penfeld settled. In trying to solve this issue, the load-bearing capacity of the Penfeld was increased but some sites remained impossible to sound as the Penfeld could not rest on the seabed for more than 5 minutes before toppling.

Reference name	Tip	Date	Hour	Lat° N	Long° E	Water depth [m]	Penetration [m]	Cause of the refusal
GAS-CPTu01-S01	E2P4	16/09/15	19h04	43,976927	31,030280	820	20,00	Inclination
GAS-CPTu01-S02	E2P4	16/09/15	22h18	43,970393	31,044035	812	0,00	Inclination
GAS-CPTu01-S03	E2P4	16/09/15	22h43	43,970247	31,043897	815	0,10	Inclination
GAS-CPTu01-S04	E2P4	16/09/15	22h43	43,970247	31,043897	815	0,20	Inclination
GAS-CPTu01-S05	E2P4	16/09/15	23h30	43,968880	31,047795	833	9,95	Inclination
GAS-CPTu01-S06	E2P4	16/09/15	00h13	43,968812	31,047727	840	10,78	Inclination

GAS-CPTu01-S07	E2P4	16/09/15	01h45	43,967163	31,051783	834	30,00	0
GAS-CPTu02-S01	E3P3	17/09/15	20h45	43,966572	30,750402	540	30,00	0
GAS-CPTu02-S02	E3P3	17/09/15	01h37	43,955600	30,763733	666	30,00	0
GAS-CPTu03-S01	E3P3	18/09/15	22h12	43,964693	31,057098	865	29,06	Inclination
GAS-CPTu03-S02	E3P3	18/09/15	00h30	43,973563	31,035988	820	2,60	Inclination
GAS-CPTu03-S03	E3P3	18/09/15	04h24	43,973777	30,996208	789	30,00	0
GAS-CPTu03-S04	E3P3	18/09/15	04h57	43,971342	30,998502	807	30,00	0
GAS-CPTu04-S01	E3P3	19/09/15	21h22	44,009608	30,959282	632	30,00	0
GAS-CPTu04-S02	E3P3	19/09/15	22h43	44,007603	30,958763	638	3,26	Inclination
GAS-CPTu04-S03	E3P3	19/09/15	22h57	44,007605	30,958803	643	30,00	0
GAS-CPTu04-S04	E3P3	19/09/15	00h57	43,997593	30,956750	640	30,00	0
GAS-CPTu04-S05	E3P3	19/09/15	2h18	43,995602	30,956750	639	30,00	0
GAS-CPTu04-S06	E3P3	19/09/15	04h49	43,991622	30,955292	661	30,00	0
GAS-Vp01-S01	Vp	20/09/15	18h12	44,009585	30,959247	655	30,00	0
GAS-Vp01-S02	Vp	20/09/15	19h35	44,007543	30,958745	661	0,18	Inclination
GAS-Vp01-S03	Vp	20/09/15	20h48	43,997682	30,958745	660	30,00	0
GAS-Vp01-S04	Vp	20/09/15	22h26	43,995522	30,956372	662	30,00	0
GAS-Vp01-S05	Vp	20/09/15	00h07	43,991768	30,955260	659	0,10	Inclination
GAS-Vp01-S06	Vp	20/09/15	00h32	43,991723	30,955157	660	30,00	0
GAS-CPTu05-S01	E3P3	21/09/15	20h40	43,938789	30,864352	786	30,00	0
GAS-CPTu05-S02	E3P3	21/09/15	22h16	43,936668	30,856118	764	10,80	Inclination
GAS-CPTu05-S03	E3P3	21/09/15	23h02	43,935917	30,852545	747	17,36	Tip resistance
GAS-CPTu05-S04	E3P3	21/09/15	00h03	43,935139	30,849321	784	30,00	0
GAS-CPTu05-S05	E3P3	21/09/15	01h33	43,933875	30,844378	815	27,82	Applied load
GAS-CPTu05-S06	E3P3	21/09/15	03h10	43,931958	30,837167	870	30,00	0
GAS-CPTu05-S07	E3P3	21/09/15	04h40	43,931402	30,835220	876	30,00	0
GAS-Vp02-S01	Vp	22/09/15	16h06	43,939172	30,865805	789	30,00	0
GAS-Vp02-S02	Vp	22/09/15	18h03	43,935902	30,852527	748	17,36	Applied load
GAS-Vp02-S03	Vp	22/09/15	19h06	43,935130	30,849323	784	30,00	0
GAS-Vp02-S04	Vp	22/09/15	20h36	43,933920	30,844465	816	27,82	Applied load
GAS-Vp02-S05	Vp	22/09/15	22h43	43,931372	30,835068	875	30,00	0
GAS-Vp02-S06	Vp	22/09/15	00h51	43,939330	30,850700	740	11,32	Applied load
GAS-CPTu06-S01	E3P3	23/09/15	23h04	43,920402	30,758882	679	30,00	0

GAS-CPTu06-S02	E3P3	23/09/15	01h05	43,926738	30,756277	646	30,00	0
GAS-CPTu06-S03	E3P3	23/09/15	2h50	43,927442	30,743163	617	30,00	0
GAS-CPTu06-S04	E3P3	23/09/15	05h08	43,943068	30,749007	612	28,90	Applied load
GAS-CPTu06-S05	E3P3	23/09/15	08h33	43,962942	30,756120	629	30,00	0
GAS-Vp03-S01	Vp	24/09/15	19h35	43,920420	30,759116	679	30,00	Inclination
GAS-Vp03-S02	Vp	24/09/15	21h17	43,926716	30,756278	642	4,64	Inclination
GAS-Vp03-S03	Vp	24/09/15	21h40	0,000000	0,000000		0,00	Inclination
GAS-Vp03-S04	Vp	24/09/15	02h40	0,000000	0,000000		0,00	Inclination
GAS-Vp03-S05	Vp	24/09/15	03h18	43,925368	30,756735	651	30,00	0
GAS-Vp03-S06	Vp	24/09/15	05h18	43,927484	30,743202	617	28,94	Applied load
GAS-Vp03-S07	Vp	24/09/15	07h41	43,943132	30,749089	613	28,76	Applied load
GAS-CPTu07-S01	E3P3	25/09/15	20h20	43,946354	30,848759	691	19,02	Applied load
GAS-CPTu07-S02	E3P3	25/09/15	21h24	43,944104	30,849139	697	30,00	0
GAS-CPTu07-S03	E3P3	25/09/15	23h07	43,939542	30,843601	788	19,60	Applied load
GAS-CPTu07-S04	E3P3	25/09/15	00h21	43,939347	30,850726	729	6,88	Pressure
GAS-CPTu07-S05	E3P3	25/09/15	00h58	43,937965	30,851792	740	17,56	Effort pointe
GAS-CPTu07-S06	E3P3	25/09/15	02h20	43,930761	30,854134	793	30,00	0
GAS-CPTu07-S07	E3P3	25/09/15	03h56	43,927638	30,854646	806	5,70	Pressure
GAS-CPTu08-S01	E3P3	26/09/15	16h12	44,002845	30,939778	611	0,10	Inclination
GAS-CPTu08-S02	E3P3	26/09/15	16h26	44,002777	30,939887	611	23,97	Inclination
GAS-CPTu08-S03	E3P3	26/09/15	17h41	44,001288	30,943658	613	30,00	0
GAS-CPTu08-S04	E3P3	26/09/15	19h28	43,997189	30,951186	603	30,00	0
GAS-CPTu08-S05	E3P3	26/09/15	20h53	43,996581	30,952040	620	30,00	0
GAS-CPTu08-S06	E3P3	26/09/15	22h44	43,991782	30,951632	651	29,34	Applied load
GAS-CPTu08-S07	E3P3	26/09/15	00h10	43,990193	30,948407	654	30,00	0
GAS-CPTu08-S08	E3P3	26/09/15	01h26	43,989516	30,949717	652	30,00	0
GAS-Vp04-S01	Vp	27/09/15	20h16	43,946487	30,848765	691	0,00	Inclination
GAS-Vp04-S02	Vp	27/09/15	21h41	43,944097	30,849168	697	30,00	0
GAS-Vp04-S03	Vp	27/09/15	23h17	43,939550	30,843623	788	16,56	Applied load
GAS-Vp04-S04	Vp	27/09/15	00h30	43,938017	30,851795	740	17,74	Applied load
GAS-Vp04-S05	Vp	27/09/15	01h42	43,936573	30,856130	764	30,00	0

Table 12: Summary of the soundings carried out with the Penfeld penetrometer. The line in grey indicates when soundings did not go deeper than 1m below seabed.

During the first dive, the piezocone E2P4 was used. Its characteristics are presented in table 13. All other CPTu were carried out using the piezocone E3P3. Comparison piezocone characteristics show that the lateral friction and pore pressure sensors of E3P3 were best suited for the very soft sediment of the Black Sea.

Piezocone	Sensor	Measurement range	Piezocone	Sensor	Measurement range
E2P4	Tip resistance	20 kN	E3P3	Tip resistance	20 kN
	Sleeve friction	10 kN		Sleeve friction	5 kN
	Pore pressure	7 MPa		Pore pressure	1.5 MPa

Table 13: Summary of the characteristics of piezocone E2P4 and E3P3.

Preliminary analysis of geotechnical and acoustic soundings

The black profiles presented in the three graphs of figure 18 illustrate a common trend to several soundings. The pore pressure profile is noisy and, since these values are used to correct measured tip resistances, the q_t profile is noisy too, particularly between 10 and 16 m depth. This noisy signal characterized by high frequency oscillations is generally observed where values of tip resistance and sleeve friction are very low. That is to say, where the sediment is very soft. The amplitude of the high frequency oscillations is lower where stiffer sediments occur as shown by the purple profiles in figure 18.

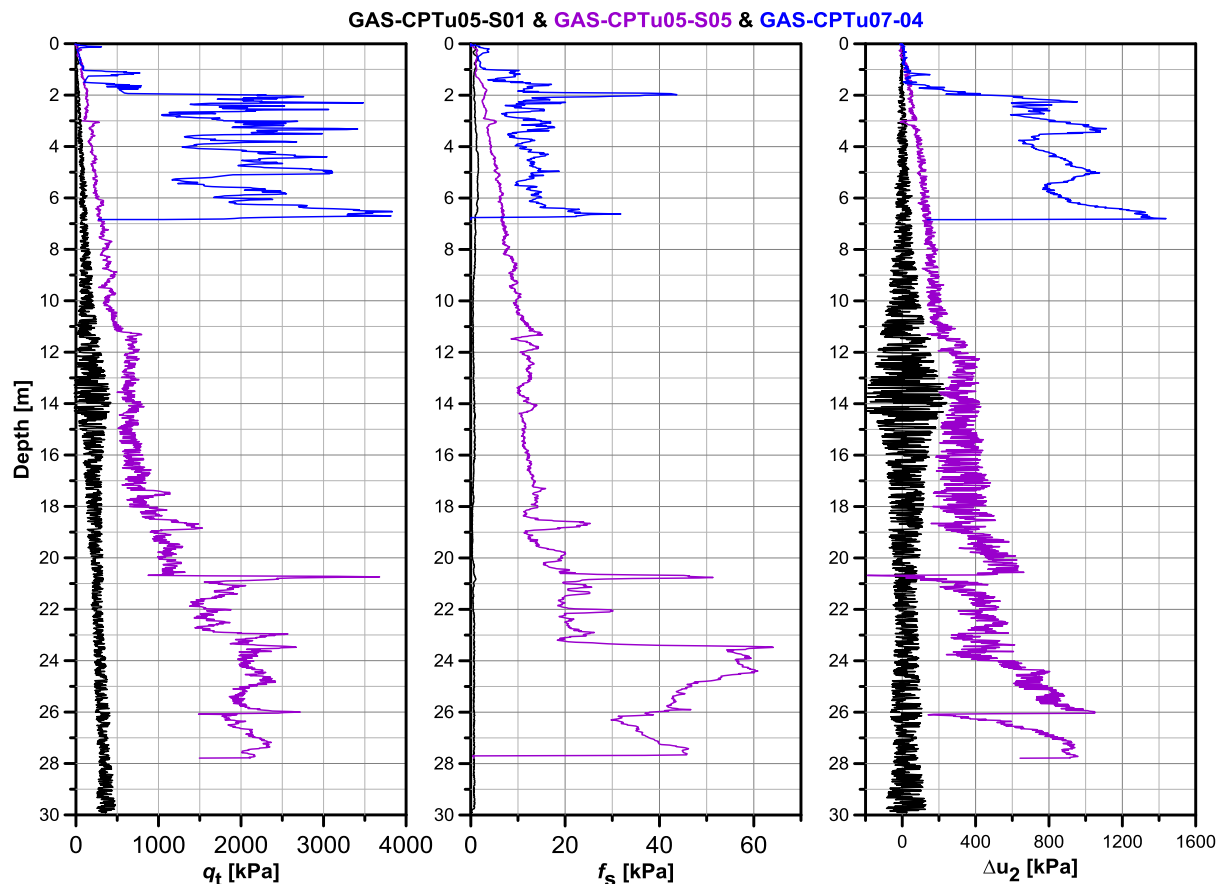


Figure 18: Comparison of piezocone soundings GAS-CPTu05-01 (black), GAS-CPTu05-05 (Purple) and GAS-CPTu07-04 (Blue).

Based on the strong difference between the black and purple profiles, it was suspected that hydrate bearing sediments occurred at site GAS-CPTu05-05. This has been supported by the difference observed between the *in situ* acoustic profiles acquired at the same location (Fig. 19).

The Vp values of profile GAS-Vp02-S04 are almost constantly above those of profile GAS-Vp02-S01 (Figure 19). The Vp values lower than 1400 m/s would be indicative for the presence of free gas. The presence of hydrates where profiles GAS-CPTu05-05 and GAS-Vp02-S01 were acquired has been confirmed by the recovery of cores GAS-CS07 and GAS-CS08. Comparison of the purple and blue curves presented in figure 18 suggested that higher quantity of hydrates occurred at site GAS-CPTu07-S04 compared to site GAS-CPTu05-S05. This was confirmed when core GAS-CS14 was recovered. Based on the criteria here mentioned, ongoing works are oriented towards inferring the presence of hydrates on *in situ* soundings when no cores could have been collected for ground truth.

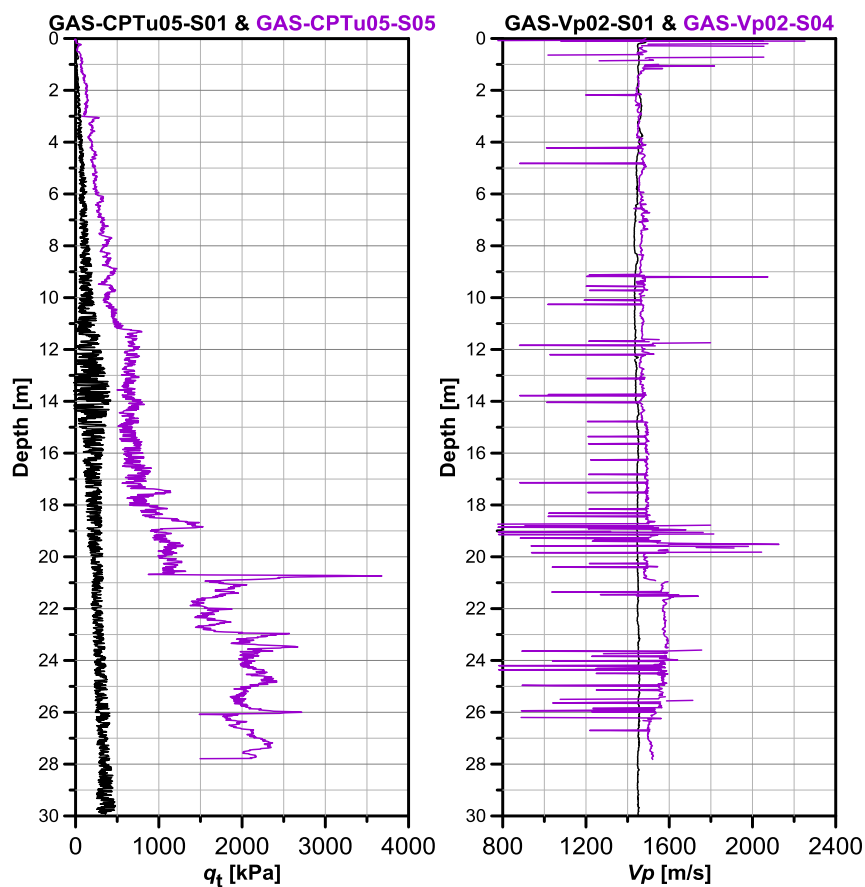


Figure 19: Comparison of piezocone and acoustic soundings at two sites.

VI.2 Pore pressure and temperature measurements with the Ifremer piezometer

Details of the Ifremer piezometer

The piezometer developed at Ifremer is a lance-like shaft with a weight on top to be free-fall deployed into the sediment (Fig. 20). The weight remains connected to the research vessel and is acoustically released and recovered once the lance has penetrated. The maximum length of the lance is 12 m. Elements containing differential pressure sensors (accuracy +/- 0.5 kPa) and temperature probes (accuracy +/- 0.05°C) can be mounted on the lance with a minimum spacing of 75 cm. Batteries allow for continuous measurements over a period of up to 3 years. In case of long-term monitoring, the buoyant data logger can be acoustically

released while the lance and sensors remain in the sedimentary column (Fig. 20). In case of short-term monitoring, a cable can be placed between the piezometer on the seabed and a buoy at the sea surface in order to recover the whole system.

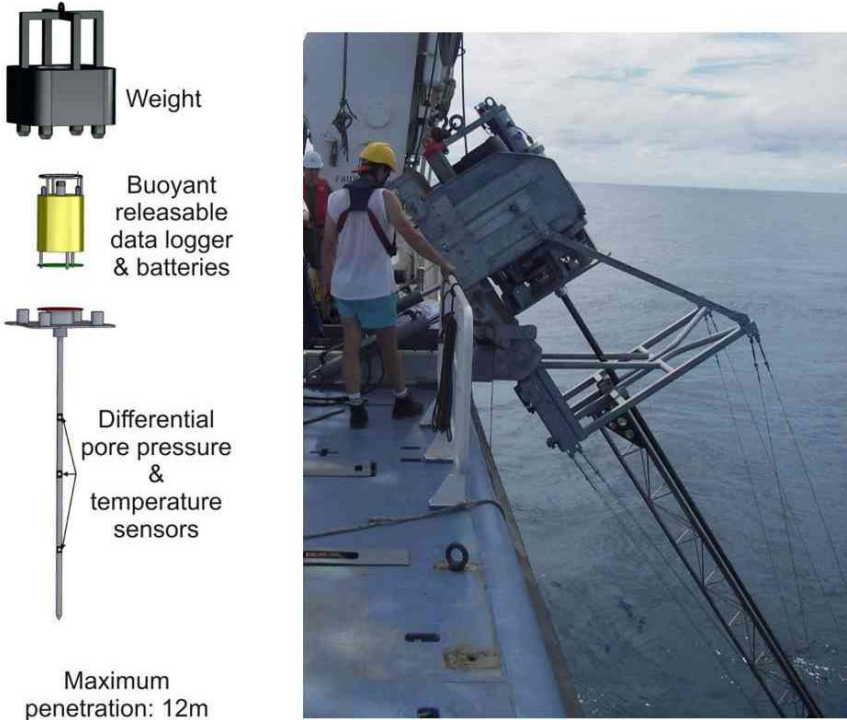


Figure 20: Illustration of the Ifremer piezometer (left) and of the way it is deployed (right).

Summary of piezometer operations

Before the GHASS cruise, two piezometers have been deployed in the Black Sea, during the MSM34 cruise in December 2013. Unfortunately, only one of them was recovered in 2015, providing information on the pressure and temperature conditions prevailing outside the hydrate stability zone (See location in Fig. 21). Based on geophysical data, *in situ* measurements and core analyses, four piezometers were deployed during the GHASS cruise for short-term measurement of pore pressure and temperature (See location in Fig. 21). Two of the sites where such measurements have been carried out have been selected for long-term monitoring over the next two years. Table 14 summarizes the characteristics of the piezometer recovered or deployed during the GHASS cruise.

Name	Sensors depth [m]	Longitude	Latitude	Water depth [m]	Deployment period	Location
Long Term						
MSM-PZ2L-01	0.81	30.415333	43.8065	394	11/12/2013	Outside the methane hydrate stability zone
	2.38				01/09/2015	
	3.93					
	5.48					
	6.28					
	7.08					
	7.88					
	8.68					
	9.48					
	9.53					

GAS-PZL2-01	0.79	30.8449655	43.933824	824.5	27/09/2015	Inside the methane hydrate stability zone
	1.59					
	2.39					
	3.94					
	5.49					
	7.04					
	7.84					
	8.64					
	9.44					
GAS-PZ2L-02	0.79	30.7571347	43.924175	587.4	28/09/2015	At the landward limit of the methane hydrate stability zone
	2.34					
	3.89					
	4.69					
	6.24					
	7.79					
	8.59					
	9.39					
	10.94					
	12.49					
Short term						
GAS-PZ2Y-01	0.79	30.7377353	44.027188	227.8	12/09/2015	Outside the methane hydrate stability zone
	2.34				17/09/2015	
	3.89					
	4.69					
	6.24					
	7.79					
	8.59					
	9.39					
GAS-PZ2Y-02	0.79	30.757079	43.924201	657.1	14/09/2015	At the landward limit of the methane hydrate stability zone
	1.59				18/09/2015	
	2.39					
	3.94					
	5.49					
	7.04					
	7.84					
	8.64					
GAS-PZ2Y-03	0.79	30.9960382	43.973803	795.1	21/09/2015	Inside the methane hydrate stability zone
	2.34				26/09/2015	
	3.89					
	4.69					
	6.24					
	7.79					
	8.59					
	9.39					
	10.94					
	12.49					
GAS-PZ2Y-04	0.79	30.8443838	43.933907	818.6	23/09/2015	Inside the methane hydrate stability zone
	1.59				26/09/2015	
	2.39					
	3.94					
	5.49					
	7.04					
	7.84					
	8.64					
	9.44					

Table 14: Summary of the characteristics of the piezometers deployed over short and long term periods.

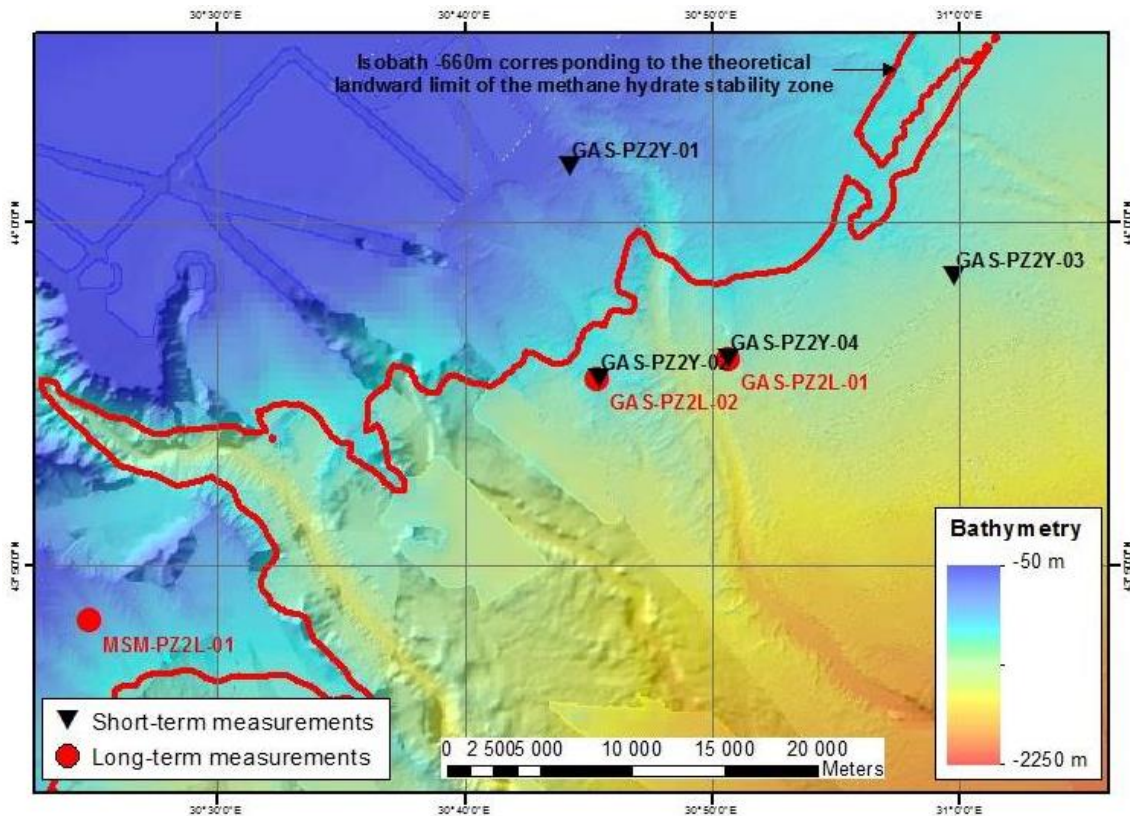


Figure 21: Bathymetric map showing the location of the piezometers deployed over short and long term periods.

1.1 Preliminary analysis of piezometer measurements

Figure 22 shows the pore pressure and temperature profiles obtained from 21 months of monitoring with piezometer MSM-PZ2L-01 outside the theoretical methane hydrate stability zone. It is noteworthy that except for the two deepest sensors, all the others have measured hydrostatic pressures (i.e. differential pressure = 0 kPa) after the excess pore pressure induced by the penetration of the lance has dissipated. The sawtooth curve obtained from the deepest sensor suggests that episodic increases in fluid pressure have been relieved upon fracturing. This has to be investigated by taking into account the fact that the temperature measured at the same depth is also that which shows the strongest change.

Figure 23 shows an example of pore pressure and temperature profiles obtained from 5 days of monitoring with piezometer GAS-PZ2L-02 at the landward limit of the methane hydrate stability zone. It illustrates a common characteristic to all short-term piezometer deployment during the GHASS cruise that is, a period of five days was not sufficient for the induced excess pore pressure to fully dissipate. Based on the shape of the pressure curves in figure 10, one may however already infer that equilibrium pressures would be above hydrostatic. This will be confirmed by applying the method proposed by Sultan and Lafuerza (2013) to extrapolate equilibrium pressure from piezometer dissipation curves.

In figure 23, one can also note that the temperatures have not varied over 5 days. When plotting these temperature values against depth (Figure 24), a thermal gradient of 134°C/km can be calculated for the upper 4 m of sediment. Such a gradient suggestive of an upward fluid flux is much higher than those around 20°/km measured at other sites where short-term piezometers were deployed.

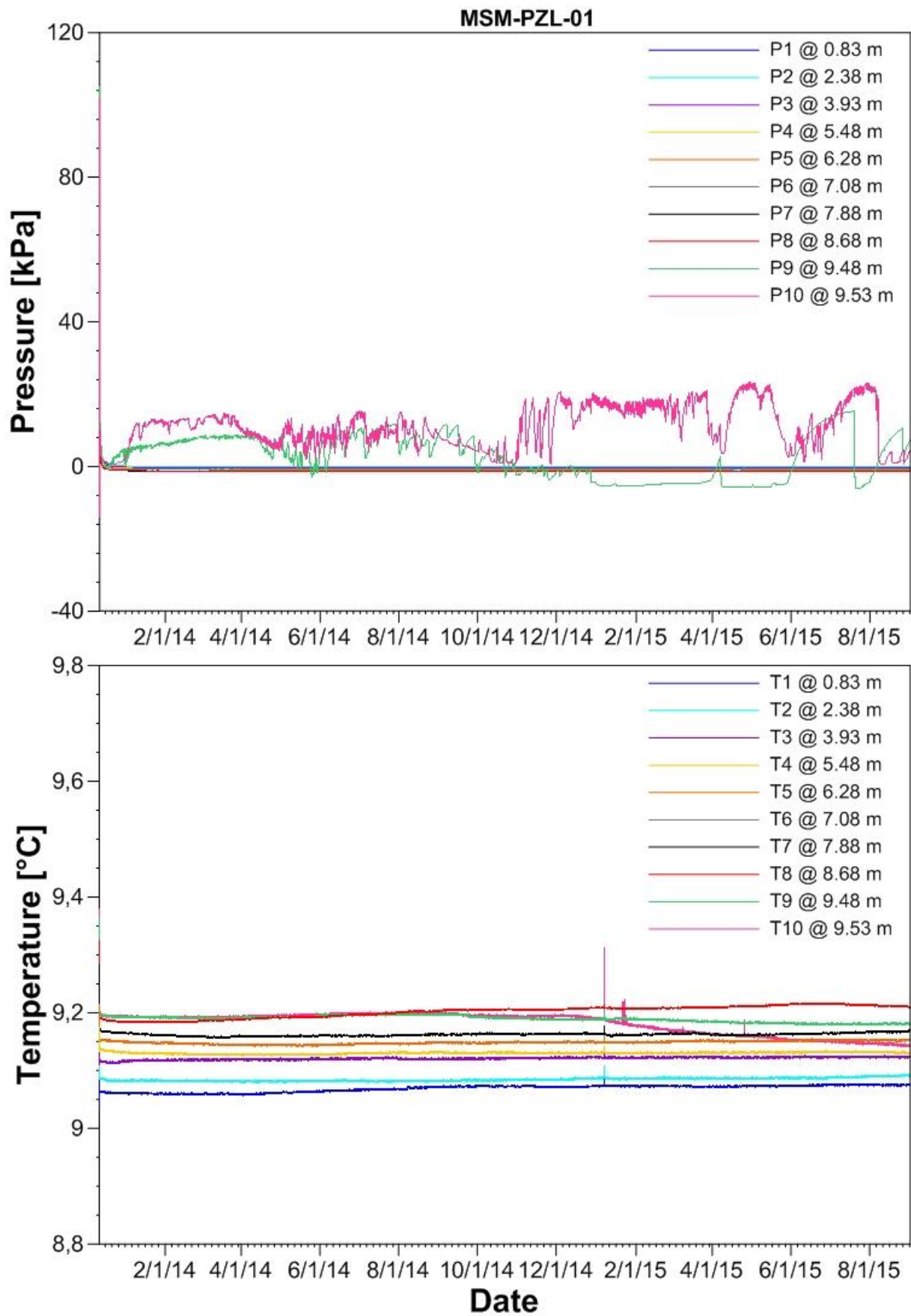


Figure 22: Differential pressure and temperature measured by piezometer MSM-PZL-01 from the 11/12/2013 to the 01/09/2015.

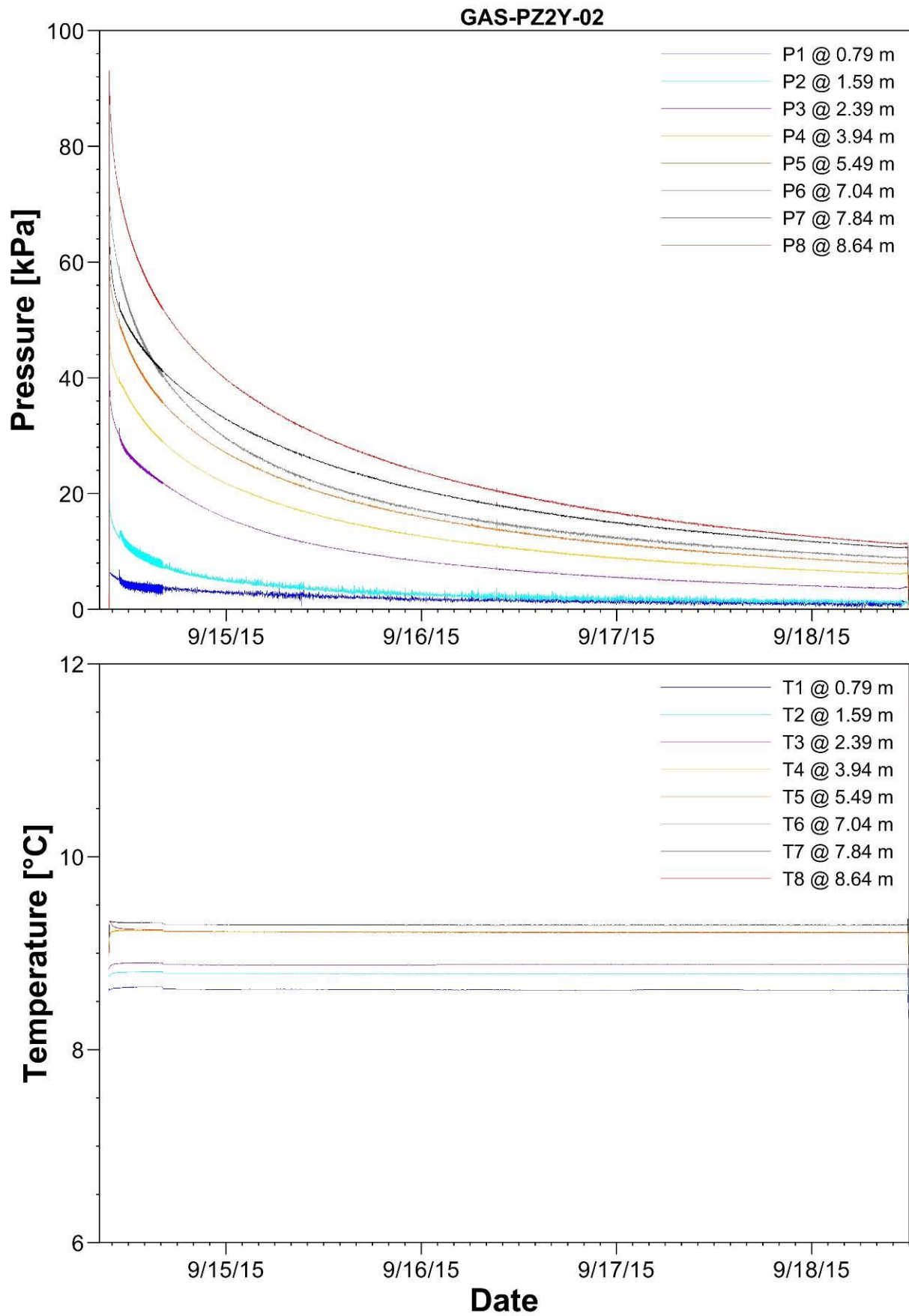


Figure 23: Differential pressure and temperature measured by piezometer GAS-PZ2Y-02 from the 14/09/2015 to the 18/09/2015.

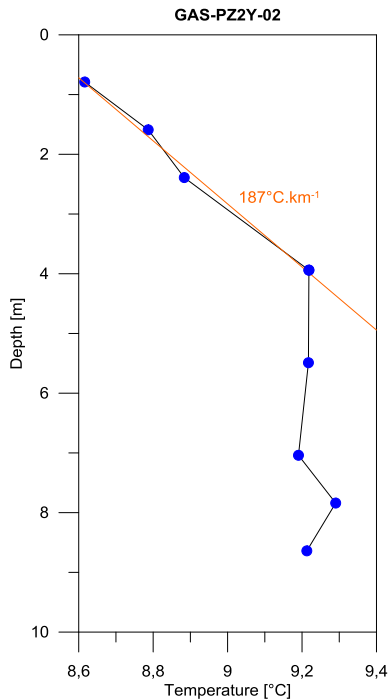


Figure 24: Plot of the temperatures measured by piezometer GAS-PZ2Y-02 against depth.

VI.3. Coring

Details of the coring system (Calypso, Interface, Gravity corer)

The Calypso piston corer of the Pp? was mainly used in undisturbed sediments (Ifremer equipment - code GAS-CS-xx). The tube lengths (6 to 36 m) and weights were defined according to target penetration. 18 Calypso cores were recovered in the GHASS areas (17 in north area and 1 in central area) from 161 to 1620 m water depth and with a length ranging between 5.6 and 33.7 m (see Table 15 and Figure 25). Except for the second core where the corer was lost on the shelf, the penetration of the Calypso was generally good and the visual quality was very good with no apparent disturbance of sediments except in gas hydrate zones.

The gravity corer (Marum equipment – code GAS-GC-xx), with a length of 3 or 5 m, is well adapted for coring in soft sediments with presence of gas hydrates at a shallow depth below the seafloor. Three gravity cores (see Table 15 and Figure 25), 0.1 to 0.5 m long, were recovered in targets suspected to contain gas hydrates and/or carbonate concretions (Crest area). The gravity corer was used with a plastic hose liner in order to allow gas hydrate sampling immediately after recovery. These hydrate samples were stored in liquid nitrogen for further analysis on land.

We have also acquired Interface cores using the Ronanberg and the Multitube Corer (see Table 15 and Figure 25).

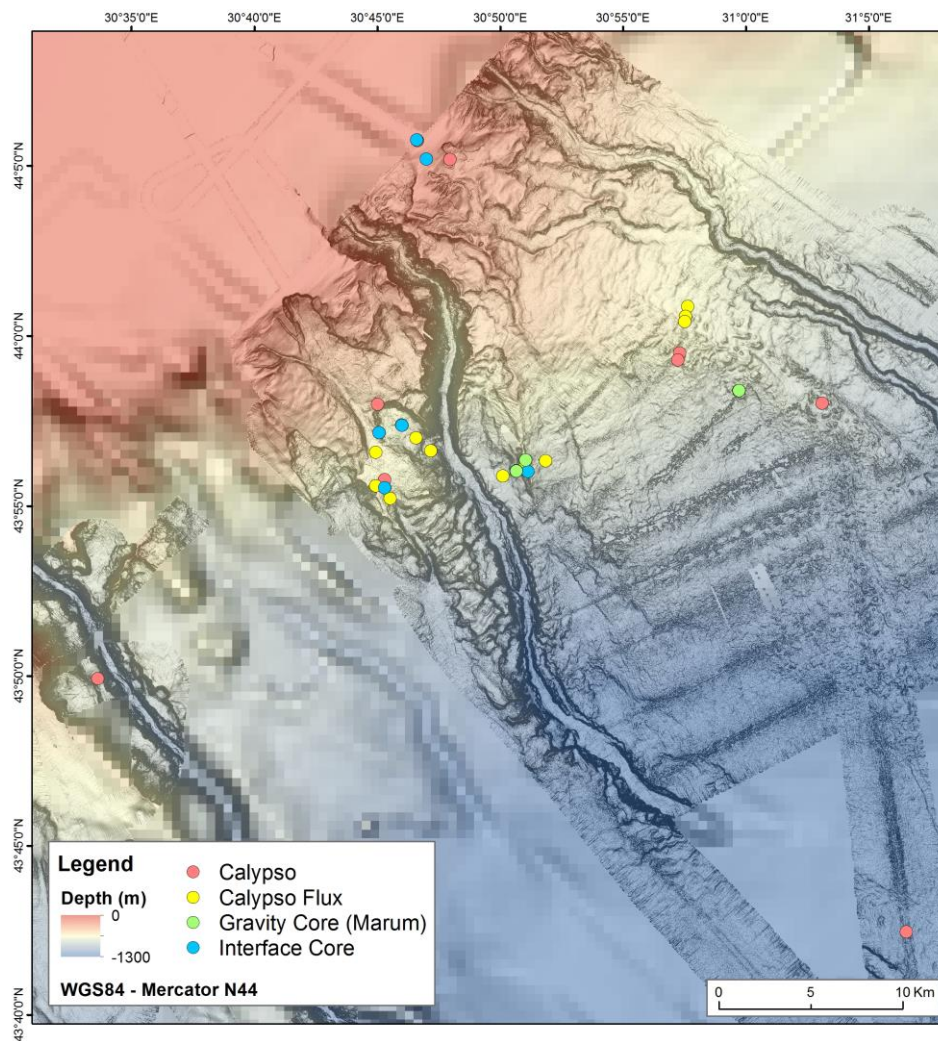


Figure 25: Bathymetry map showing the location of the cores.

Core	Date	Time	Lat.	Long.	Depth, m	Objective
Calypso						
GAS-CS01	16/09/2015	15:27	N44°05,188	E30°47,961	240	North area: Sedimentological core (upper slope)
GAS-CS02	17/09/2015	11:29	N44°05,736	E30°46,648	161	North area: Sedimentological core (shelf) = Loss of the corer
GAS-CS03	19/09/2015	09:42	N43°58,03	E31°03,107	842	North area: Gas hydrates (instabilities, HG and free gas)?
GAS-CS04	20/09/2015	10:05	N43°42,454	E31°06,541	1620	North area: Sedimentological core in distal environment
GAS-CS05	20/09/2015	15:39	N43°58,394	E30°59,735	794	North area: HG
GAS-CS06	21/09/2015	05:35	N43°59,4985	E30°57,3159	650	North area: HG
GAS-CS07	23/09/2015	03:24	N43°56,0348	E30°50,6635	822	North area (Crest): Gas and HG (GHSZ) - GH found
GAS-CS08	23/09/2015	17:55	N43°56,0348	E30°50,6635	821	North area (Crest): Gas and HG (GHSZ) - GH found
GAS-CS09	24/09/2015	13:22	N44°05,752	E30°46,607	161	North area: Sedimentological core (shelf) ~100 m NW of the CS02
GAS-CS10	24/09/2015	17:07	N43°55,540	E30°45,299	651	North area: right above the vertical BSR (Empty Core)
GAS-CS11	25/09/2015	11:55	N43°49,927	E30°33,632	840	Central area: Sedimentological core (Canyon activity)
GAS-CS12	26/09/2015	08:23	N43°57,994	E30°45,020	547	North area: Slide studies by Geomar (Upwar the scarp)
GAS-CS13	26/09/2015	13:50	N43°59,298	E30°57,234	660	North area (pingoe): Gas hydrates?

GAS-CS14	27/09/2015	04:48	N43°56,361	E30°51,044	738	North area (Crest): Gas hydrates? - GH found
GAS-CS15	27/09/2015	17:24	N43°55,540	E30°45,299	646	North area: right above the vertical BSR (Empty Core)
GAS-CS16	28/09/2015	05:37	N43°57,3778	E30°46,0132	685	North area: Slide studies by Geomar (Within the scarp)
GAS-CS17	28/09/2015	21:51	N44°00,5766	E30°57,557	650	North area (pingoe): Gas hydrates?
GAS-CS18	29/09/2015	22:51	N43°55,777	E30°45,301	638	North area: right above the vertical BSR

Core	Date	Time	Lat.	Long.	Depth, m	Objective
Calypso flux						
GAS-CSF01	18/09/2015	13:27	N43°55,225	E30°45,530	688	North area: right above the vertical BSR
GAS-CSF02	18/09/2015	16:07	N43°55,599	E30°44,939	655	North area: Upward a headwall scarp
GAS-CSF03	18/09/2015	17:32	N43°56,584	E30°44,939	617	North area: Slide studies by Geomar
GAS-CSF04	23/09/2015	06:46	N43°56,330	E30°51,859	793	North area: Gas hydrate system (Crest)
GAS-CSF05	23/09/2015	07:57	N43°56,109	E30°50,960	785	North area: Gas hydrate system (Crest)
GAS-CSF06	23/09/2015	08:40	N43°56,035	E30°50,666	821	North area: Gas hydrate system (Crest)
GAS-CSF07	23/09/2015	09:36	N43°55,886	E30°50,113	871	North area: Gas hydrate system (Crest)
GAS-CSF08	27/09/2015	13:05	N43°56,631	E30°47,186	784	North area: Slide studies by Geomar
GAS-CSF09	27/09/2015	14:07	N43°57,006	E30°46,578	727	North area: Slide studies by Geomar
GAS-CSF10	27/09/2015	15:08	N43°57,385	E30°46,001	676	North area: Slide studies by Geomar
GAS-CSF11	28/09/2015	17:25	N44°00,871	E30°57,643	660	North area: Pingoos
GAS-CSF12	28/09/2015	18:16	N44°00,576	E30°57,557	650	North area: Pingoos
GAS-CSF13	28/09/2015	18:55	N44°00,426	E30°57,516	653	North area: Pingoos

Core	Date	Time	Lat.	Long.	Depth, m	Objective
Interface						
GAS-IS01	17/09/2015	16:06	N43°57,378	E30°46,012	676	North area: Slide studies by Geomar (within the scarp)
GAS-IS02	17/09/2015	17:22	N43°57,156	E30°45,082	635	North area: Slide studies by Geomar
GAS-IS03	17/09/2015	18:23	N43°57,156	E30°45,082	635	North area: Slide studies by Geomar
GAS-IS04	19/09/2015	14:54	N43°58,394	E30°59,734	794	North area: Pingoos
GAS-IS05	20/09/2015	14:16	N43°58,397	E30°59,720	796	North area: Pingoos
GAS-IS06	21/09/2015	07:52	N43°56,021	E30°51,140	735	North area: Gas hydrate system (Crest)
GAS-IS07	21/09/2015	08:43	N43°56,357	E30°51,0447	731	North area: Gas hydrate system (Crest)
GAS-IS08	21/09/2015	12:59	N43°56,036	E30°50,667	818	North area: Gas hydrate system (Crest) = Bubbles and GH?
GAS-IS09	24/09/2015	11:41	N44°05,191	E30°47	242	North area: Sedimentological core (upper slope at the same place of CS01)
GAS-IS10	24/09/2015	12:30	N44°05,752	E30°46,607	162	North area: Sedimentological core (shelf at the same place of CS02)
GAS-IS11	27/09/2015	06:44	N43°56,037	E30°50,663	812	North area: Gas hydrate system (Crest)
GAS-IS12	29/09/2015	01:22	N43°55,540	E30°45,299	651	North area: right above the vertical BSR

Core	Date	Time	Lat.	Long.	Depth, m	Objective
Gravity core						
GAS-GC01	19/09/2015	13:08	N43°58,3944	E30°59,7349	794	North area: Pingoos
GAS-GC02	21/09/2015	11:44	N43°56,357	E30°51,0447	755	North area: Gas hydrate system (Crest)
GAS-GC03	22/09/2015	10:22	N43°56,0348	E30°50,6635	815	North area: Gas hydrate system (Crest) - GH found

Table 15: Summary of the core detail.

Details of the analysis made onboard (Tab. 16)

Physical properties of the cores were determined onboard, on whole sections, by measuring the P-wave velocity, gamma-ray attenuation density and magnetic susceptibility every 1 cm using a 'Geotek Multi Sensor Core Logger' (MSCL). X-ray radiograph analyses were performed onboard on whole sections using a 'Geotek MSCL-XCT'. Core sections were then opened, photographed at very-high resolution and described in order to produce lithological logs. Shear resistance of sediment was investigated at about 50 cm interval using a scissometer, and discrete sediment samples were taken to measure water content for useful comparison with in-situ (Penfeld) geotechnical measurements. Finally, bulk intensity of major elements of the cores was analyzed using an Avaatech XRF core scanner (Rhodium source). XRF data were collected every 1 cm along the entire length of the cores, with a count time of 10 s, by setting the voltage to 10 kV (no filter) and 30 kV (Pd thick filter) and the intensity to 600 μ A and 1000 μ A, respectively. In addition, some intervals were analyzed every 1 mm (count time of 30 s, voltage of 10 kV, and intensity of 1000 μ A).

ID-CORE	MSCL	CT-SCAN	OPENING	PHOTOGRAPHS	DESCRIPTION	SCISSOMETER	WATER CONTENT	XRF
GAS-CS-01	X	X	X	X	X	X	X	X
GAS-CS-02	NO DATA							
GAS-CS-03	X	X	X	X	X	X	X	X
GAS-CS-04	X	X	X	X	X	X	X	X
GAS-CS-05	X	X	X	X	X	X	X	X
GAS-CS-06	X	X	X	X	X	X	X	X
GAS-CS-07	X	X	X	X	X	X	X	X
GAS-CS-08	X	X	X	X	X	X	X	X
GAS-CS-09	X	X	X	X	X	X	X	X
GAS-CS-10	NO DATA							
GAS-CS-11	X	X	X	X	X	X	X	X
GAS-CS-12	X	X	X	X	X	X	X	X
GAS-CS-13	X	X	X	X	X	X	X	X
GAS-CS-14	X	X	X	X	X	X	X	X
GAS-CS-15	NO DATA							
GAS-CS-16	X	X						
GAS-CS-17								
GAS-CS-18								

 will be done in 2016 (first semester)

Table 16: Summary about the analysis made onboard on the calypso cores

VI.4. Heat flux measurements

The geothermal gradient is measured using temperature sensors fixed at specific intervals along the pipe. Seven probes are fixed on supports welded helically around the pipe (Fig. 26). An accelerometer, fixed to the left, measures the acceleration of the core drill during penetration. The length of the pipe of the coring system used to measure the geothermal gradient is 12 m.

After penetration, the pipe is held driven into the sediment for 10 minutes to measure the geothermal gradient. During this time, the sensors record the return to the equilibrium temperature within the sediment to their respective depths. However, the equilibrium temperatures are approached but not reached. They are determined by the asymptotic values estimated from the temperature curves recorded between the penetration and extraction of the coring system. During the descent of the pipe within the water column, we carried out two long plateau (150 and 70 m above the bottom) to obtain an inter-calibration of the probes (Fig. 27). Figure 25 shows the location of the targets for the flux measurements.

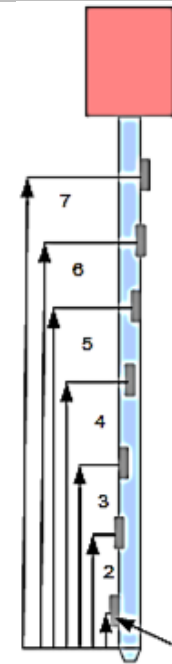


Figure 26: Coring system.

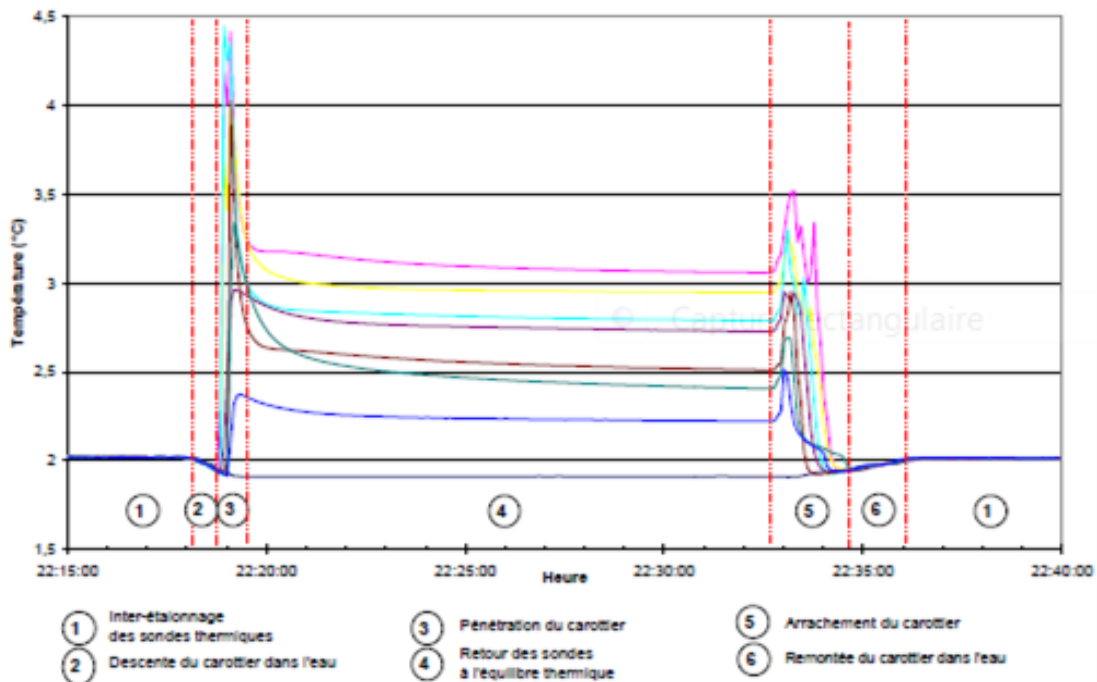


Figure 27: Example of temperature curve function of the time.

The thermistor used in the temperature measurement is positioned halfway along the pipe (Fig. 28). The electronic system and the memory are contained in the cylindrical box. The thermal probes thus formed temperature sensors are fixed on supports which hold them at 7 cm from the wall of the pipe in order to avoid the measurement artefact linked to the temperature disturbance introduced by the presence of the pipe within the sediment.



Figure 28: VHP probes in its support welded to the pipe of the coring system.

VI.5. Anitra deployment

The Anitra station, equipped with an ADCP current meter 75 kHz and a particulate trap (12 buckets), was deployed in the Danube canyon on 09/01/2015 at 4:02 p.m. at coordinates N43°50.1885; E30°34.3597 (BUC positioning). The recovery took place on 09/25/2015 at 00:30 p.m.

The samples recovered in the buckets are currently being analyzed, in particular for the quantification of inputs in organic matter. The current meter was programmed to describe the water column of 300 meters within 59 discrete layers of 5 m thick with the exception of the first layer of 13.30 m thick.

The observed velocities are low throughout the period (<10 cm / s) with a direction hovering around the main direction of the canyon. The acquired velocities have good quality on the first 200 m. The hundred meters near the seafloor seems to disrupt the quality of measurements with a poor level of the quality (Fig. 29).

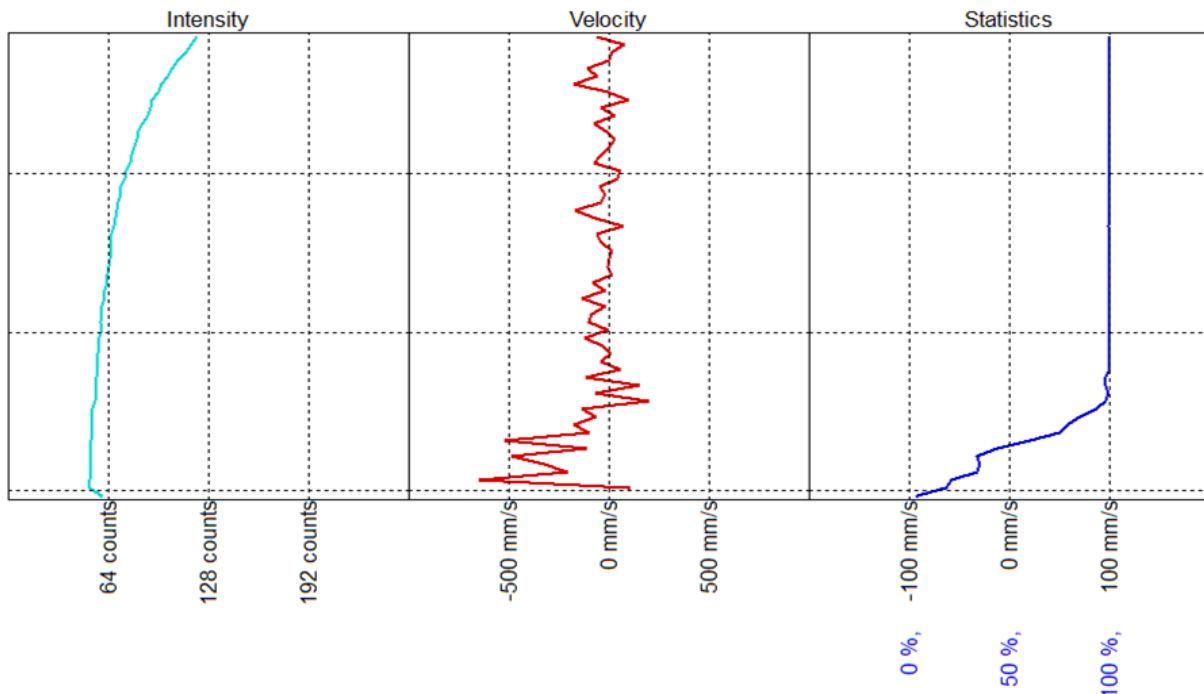


Figure 29: Profiles of the intensity of the received signal, the velocity profile, and the measurement quality. The velocity characterized the water column is low without vertical structure but the measures seem deteriorated close to the seafloor. Indeed, the basal layer (between 50 and 100 m thick depending on the time) seems to attenuate the intensity of the signal.

During the acquisition period, the bottom currents do not show vertical structure. Near the seafloor, we might suspect very charged suspensions as the cause of poor return of the acoustic signal. The intensity profile appears to decrease sharply 100 m close to the seafloor. The received intensity remains very low for a good quality signal. The thickness of this layer varies between 50 and 100 m.

VI.5. Water Column Survey – CTD-rosette

Objectives

In recent years, the characterization of gases emitted into the water column has become a focus of extensive research. It provides both useful information on the fate of methane and allows to quantify the ocean's contribution to climate change, and consists of a promising detection method with possible applications to the hydrocarbon industry.

The primary objective of the study of the water column as part of the GHASS cruise was to couple acoustic surveys with geochemistry in order to describe the spatial dynamics of gas plumes in the Black Sea. Thus, extensive acoustic surveys were carried out to map out the acoustic anomalies in the Romanian sector of the Black Sea. This was followed by the deployment a multisensory-equipped CTD-Rosette at two selected acoustically active sites to better understand the chemical nature and the fate of the gases forming plume above seep areas.

The latter operation was also an opportunity to test and validate the use of *in situ* chemical sensors for dissolved methane measurements in the water column, together with water sampling for on board methane analysis.

Methodology - Tools

The CTD-rosette package consisted of a Seabird 911+ fitted with 24 Niskin bottles and various sensors for conductivity, temperature, pressure, and a Seapoint turbidity Meter.

The package was completed with three sensors and analysers for dissolved methane measurements: GASPARD (*in situ* mass spectrometer), MESSEA (Methane Sensor for the Sea) and a METS sensor from Franatech.

An important feature of the package was the implementation of an acoustic transponder allowing precise positioning of the CTD-rosette in the water column relative to the ship position. It was scheduled to exclude MESSEA deployment for the first dive, in order to privilege testing the waterproof capability of its new housing before any *in situ* use. Unforeseen electrical issues led us to finally operate only GASPARD during the vertical casts in the same configuration as during the STORM cruise (January 2015) on board the R/V l'Atalante. The ISMS GASPARD is currently regarded as promising technology for real-time monitoring of gas plumes. Data from GASPARD were transmitted via a self-supporting electro-cable to the SBE11+ Deck Unit and computed using a homemade software, while energy for GASPARD was provided by a Li-ion battery pack specifically designed to meet the power requirements of the instrument for a dive (5-hour dive). The homemade software was designed not only to collect and compute the data from GASPARD but also to transmit orders such as starting the instrument and firing the Niskin bottles. Real-time data from the CTD and Turbidity sensors were transmitted to the same Deck Unit and computed using the SeaSave software with the usual data correction recommended by Seabird.

Methodology - Profiling and sampling

Two strategies were used to characterize the distribution of the gases throughout the water column above seep areas. The first one was to apply the tow-yo technique (Figure 30) above a seep area where several gas sources were spotted from the acoustic survey.

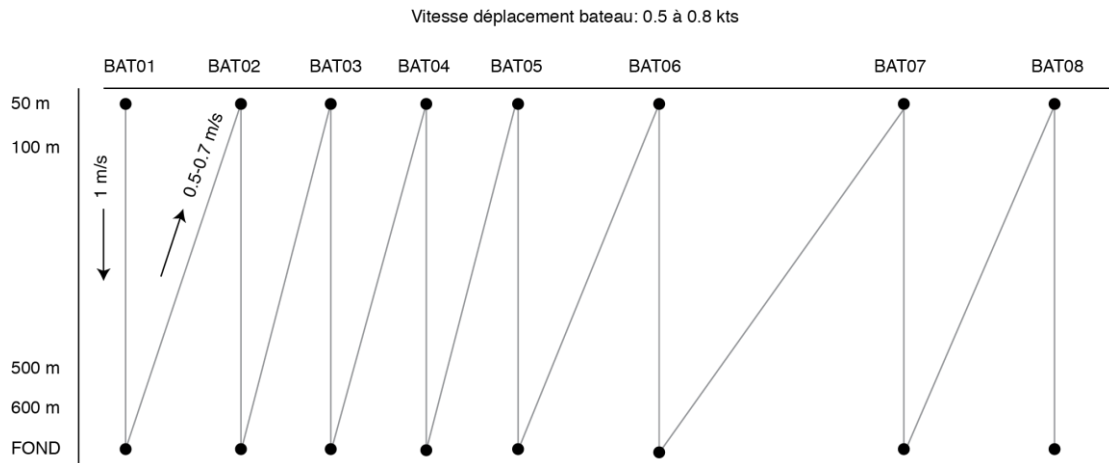


Figure 30: In situ measurements and water sampling strategy for GAS-HY03

The second strategy consisted in simple vertical casts at different locations close to the gas bubble emission areas. Locations were chosen according to the currents.

During the CTD-rosette hydrocasts, water was sampled at different depths on the way up for dissolved methane measurements. Analyses were performed as soon as the samples were recovered, using the purge-and-trap technique followed by GC-FID measurements.

List of operations

GAS-HY01: first deployment of the CTD-rosette, aborted after the first profile due to technical problems with GASPARD (loss of communication). Nevertheless, 5 water samples were taken for dissolved-methane analysis at 627, 577, 500, 100, 50 m depth.

GAS-HY02: second deployment of the CTD-rosette. This deployment aimed at testing the communication with the CTD after several isolation defaults. 4 water samples were taken at 100, 75, 50, 25 m depth.

GAS-HY03: third deployment of the CTD-rosette (tow-yo) on the same seep area as for GAS-HY01. The operation lasted 4h30, with a successful use of GASPARD. In addition, 24 water samples were taken.

GAS-HY04 and GAS-HY05: The fourth and fifth deployments of the CTD-rosette were coupled and performed on the same sites. They consisted of vertical profiles, where 24 samples each were taken.

Preliminary results

From a technological point of view, we have validated the use of the *in situ* mass spectrometer GASPARD for water column measurements in a highly methane concentrated environment. The combination of both *in situ* chemical measurements and acoustic surveys allowed a concise description of the geochemical processes in the water column, which underpins the relevance of this strategy to intercept methane plumes and to understand the behaviour of methane in the water column above seep areas.

Both GASPARD data and water samples confirm the very high concentration of dissolved methane throughout the water column (Fig. 31), with values up to 12 μM in the bottom waters close to the seafloor. GASPARD data show a stepwise increase of methane concentrations with depth. One important feature which can be seen from the resulting profile is the significant increase in methane concentrations just below the halocline (~100 m depth).

It appears from the first data that concentrations in the upper layers are still very high (100 nM at 50 m depth). This means that methane emissions at 700 m depth have an impact on the upper layers and would contribute to the global methane emissions into the atmosphere.

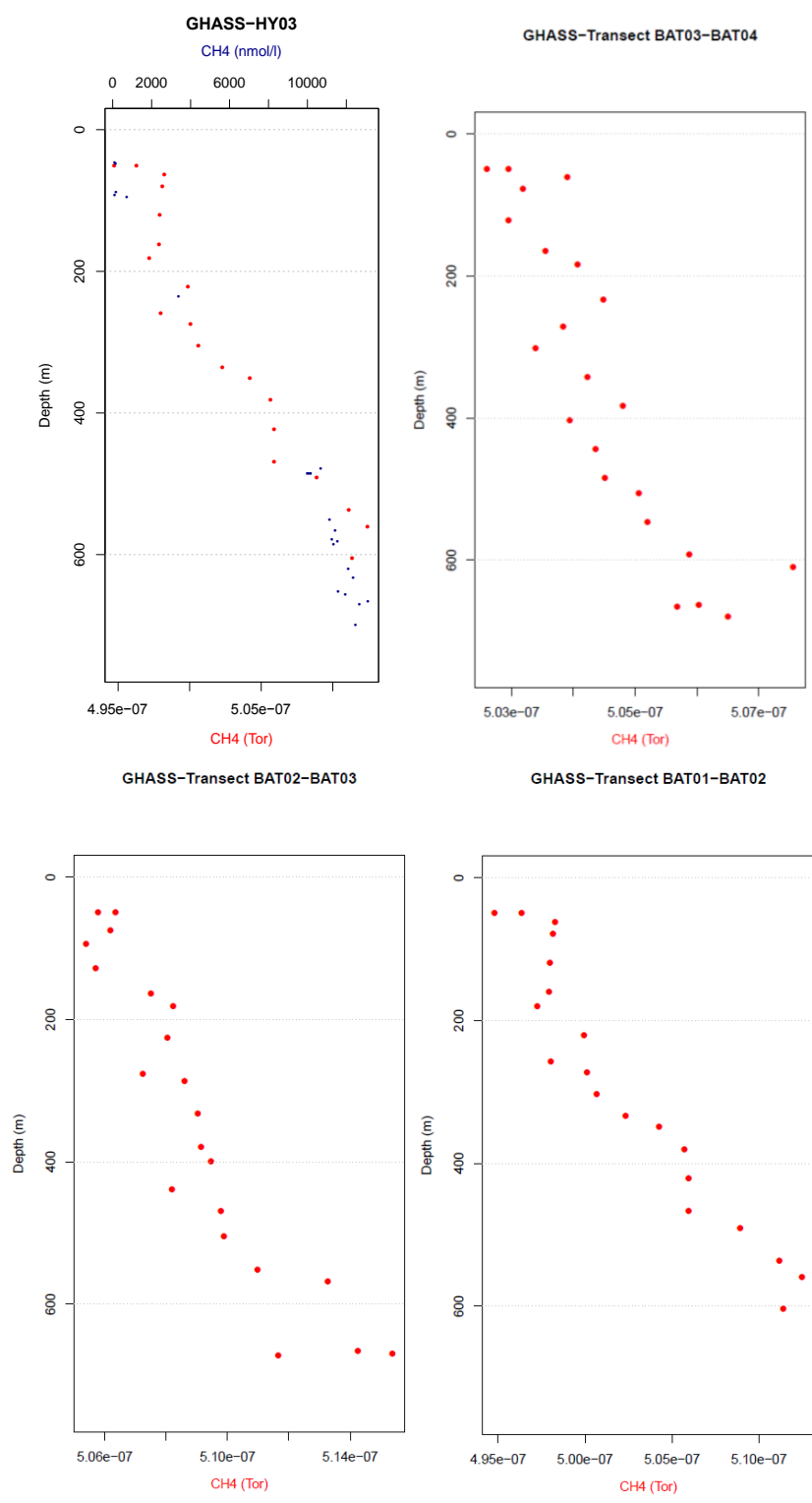


Figure 31: Methane profiles in the water column (red: in situ data from GASPARD in Tor; blue: composite profile from all water samples). Below: vertical methane profiles obtained with GASPARD along GAS-HY03 transects.

VII. ANALYSIS ON PISTON CORES

VII.1. Geotechnical and acoustic measurements on piston cores

Detail of geotechnical and acoustic measurements performed onboard

Eleven piston cores collected with the Calypso corer were subjected to onboard laboratory measurements. Before splitting, the bulk density and compressional wave velocity (V_p) of each of these cores was measured with the GEOTEK multi-sensor core logger. Based on the analysis of density and V_p profiles, some samples were selected and kept in a cold chamber to perform oedometer and triaxial tests onshore. The remaining core sections were split in two halves. Thereafter, shear strength measurements were carried out using a vane shear device, 15 cm each, when the sediment was of clayey nature. Peak and residual strengths were thus determined. These were completed by acoustic measurements performed with a sonic fork with similar characteristics to that used with the Penfeld (1 MHz, 7 cm spacing between source and receiver). In addition, the water content was determined every 30 cm by weighing samples before and after 24h in an oven at 105°C.

Preliminary analysis of the geotechnical and acoustic measurements

Figure 32 shows a synthesis of all measurements carried out on core GAS-CS01 which aimed at being a reference core as it was collected outside the areas where free gas and gas hydrates were suspected based on geophysical grounds. However, the geotechnical and acoustic profiles obtained on this core share similarities with most of the cores retrieved. Those similarities result from the damaging effect of gas charging. This is most markedly illustrated in figure 32 by a drop in V_p measured with the MSCL, from values around 1450 m/s to values around 1250 m/s below 6 m depth. On core GAS-CS01 as on the majority of other cores, the sonic fork could not measure V_p deeper than this transition. This transition also correlates with a marked change of the slope the undrained shear strength value follows. From figure 5, the steeper slope below 6 m can be ascribed to the weakening of sediments upon gas exsolution.

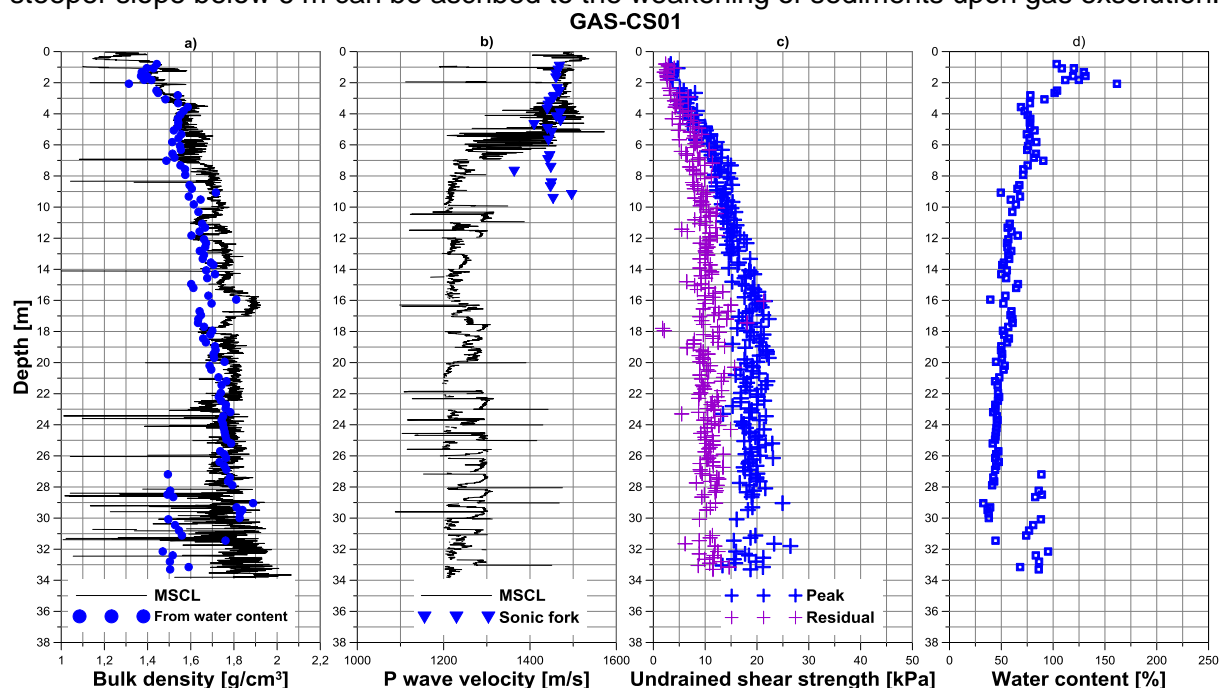


Figure 32: Synthesis of the geotechnical and acoustic data obtained on core GAS-CS01.

Figure 33 shows the synthesis of the geotechnical and acoustic data obtained on core GAS-CS07 from which hydrates were recovered. The density and shear strength values of this core are markedly lower than those of core GAS-CS01. This is taken as evidence that upon core

recovery, gas hydrate dissociation induces further severe damage to sediment properties than gas exsolution.

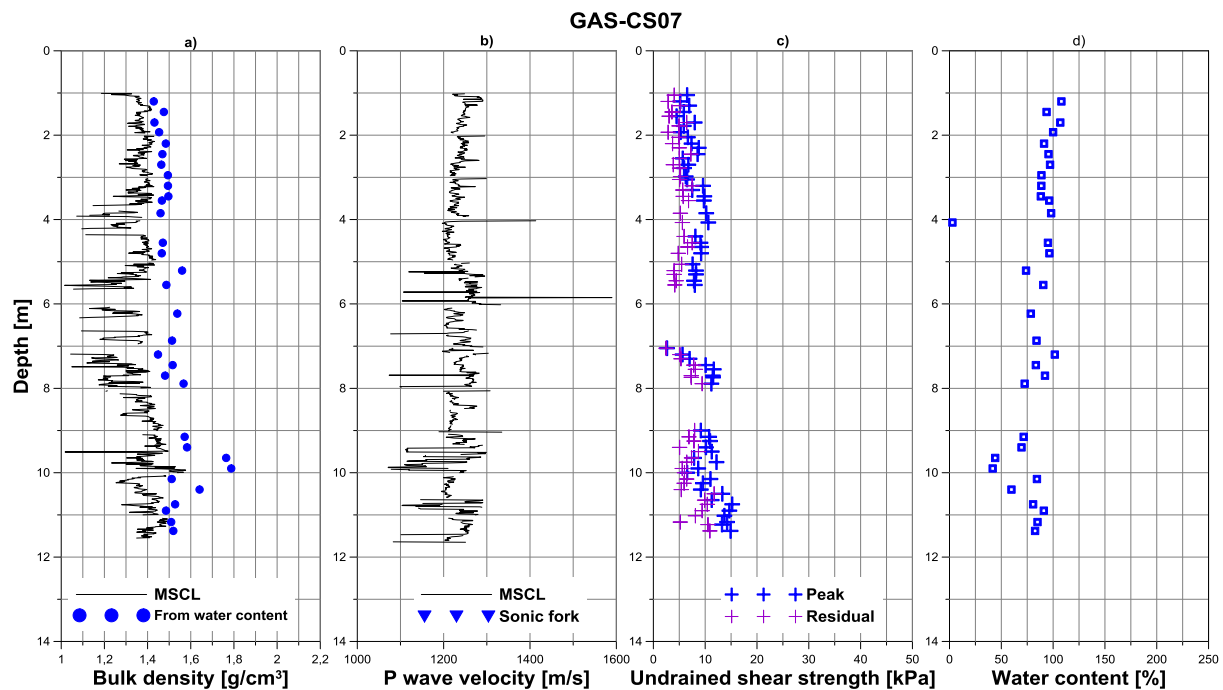


Figure 33: Synthesis of the geotechnical and acoustic data obtained on core GAS-CS07.

VII.2. Geochemistry analysis

Pore fluids and sediments: Sampling, storage and onboard analyses

The Black Sea is the largest anoxic basin on earth. It is connected to the Atlantic ocean with the Marmara and the Mediterranean Seas, and is characterized by two water masses. A salty water mass at the bottom supplied from the ocean, and nearly fresh water mass delivered by the connected rivers.

Our investigated area is located in the Romanian water sector, near the Danube canyon, where evidence of sedimentary instabilities, mainly landslides, has been observed from the MSM-34 cruise in 2013. Previous study from acoustic surveys has shown that this area is characterized by a large number of widespread gas expulsion sites at the seafloor, bubbling up to several tens to hundreds of meters into the water column. This is the expression in the water column of intense fluid migration within the anoxic Black Sea sediments. Occurrence of multiple BSRs, indicative of the presence of gas hydrates has also been revealed from seismic surveys, although gas hydrates have not been collected in this sector yet. Indirect evidence (geochemical proxy) may also be used to detect the occurrence of hydrates within the sediment. For instance, hydrate formation is usually accompanied by chloride enrichment of pore fluids, while negative chloride anomalies are indicative of hydrate dissociation (Torres et al., 2004).

In such anoxic marine sediment, there are two major biogeochemical processes responsible for the sulfate consumption: the mineralization of particulate organic matter and the anaerobic oxidation of methane (AOM) (Borowski et al., 1996; Froelich et al., 1979; Meister et al., 2013; Niewohner et al., 1998; Reeburgh, 1976; Regnier et al., 2011; Wallmann et al., 2006).

Thus, the dissolved-sulfate and methane profiles are also useful in terms of identifying the methane-bearing zone, and reciprocally the methane-free zone, within the sedimentary column for its depletion to zero corresponds to the sulfate methane transition zone (SMTZ) (Bhatnagar et al., 2008; Bhatnagar et al., 2011; Pohlman et al., 2008). Anaerobic oxidation of methane

(AOM) coupled with the sulfate-reduction reaction generally occurs at this horizon such as (Boetius et al., 2000; Joye et al., 2004; Orcutt et al., 2004):



Besides the hydrate/ methane-involving processes, pore fluids are also fingerprinted by other biogeochemical processes like authigenic mineralization and mineral dissolution. These processes can locally change the pore-fluid chemistry, and therefore strongly shape the profile of several dissolved elements with depth.

The objective of the present study is to investigate the geochemical properties of pore fluids and gas hydrates which are recovered by using two different coring techniques (gravity corer and Calypso corer). Thus, the analyses of the collected samples will be carried out in order to (1) determine the concentrations of major elements such as sulfate, chloride, sodium, potassium, magnesium and calcium, as well as trace elements (2) identify the dissolved hydrocarbons (3) measure the strontium isotope ratios and the isotopic composition of carbon for methane, and possibly carbon dioxide.

Measurements of alkalinity, ammonium as well as the profiles for sulfate and chloride were carried out on board. Thus, they provided useful information on both hydrate and methane occurrence zones.

Finally, the resulting dataset from all analyses will provide insights into the geochemical dynamics of the studied area, *i.e* will allow a fair evaluation of the spatial distribution of the hydrates, dissolved hydrocarbons and eventually free gas as well as the zonation of the different biogeochemical processes which take place in the first tens of meters within the sedimentary column.

Sampling and analytical methods

- Offshore sampling methods

During the cruise, the coring location was chosen from previous Penfeld measurements and seismic surveys. This strategy allows critical discussion of the investigated area by comparing data from different disciplines. Sediment cores were sampled for pore-fluid analyses immediately upon recovery. Pore-fluid was sampled using Rhizon samplers as long as the sediment was soft enough to insert the plastic tip of the sampler. Rhizon samplers (CSS-F 5/ 10 cm; Rhizosphere Research Products, Netherlands) is a narrow elongated cylindrical filter (0.2 µm pore size; 5 cm long; 130 µL volume) with a stiff plastic core (Seeberg-Elverfeldt et al., 2005). Before their application, these were conditioned for several hours in distilled water ("MilliQ"). Furthermore, pore-fluids of gravity-cores which consist of plastic bags instead of liners were sampled on open sediments.

Rhizon samplers draw fluid from sediment under vacuum, which is applied by attaching Rhizon samplers to 20 mL or 10 mL all-plastic syringes, pulling the plunger back, and bracing it with a small wooden stick. The pore-fluid was then collected in the syringe. The sampling took several hours by collecting pore-fluid, but no more than 12 hours. Usually, one to three Rhizon samplers were set into a 1m-length core liner collecting a maximum volume of 28 mL pore-water.

Sediment samples were also taken for chemical and mineral composition by XRF and XRD, respectively.

Chronological operations	Coordinates	Total sample number	Onboard analyses			Samples and splits to	
			Alkalinity	Sulfate/ Chloride	Methane	Brest	Kiel
GAS-CS01	N44°05,188; E30° 47,961	27		x	x	x	
GAS-CS03	N43°58,030; E31° 03,107	38		x	x	x	x

GAS-CS05	N43°58,3944; E30°59,7349	24		x	x	x	x
GAS-CS06	N43°59,4985; E30°57,3139	24		x	x	x	x
GAS-CS07	N43°56,048; E30°50,6635	34		x	x	x	x
GAS-CS08	N43°56,048; E30°50,6635	27		x	x	x	x
GAS-CS11	N43°49,927; E30°33,632	25		x	x	x	x
GAS-CS12	N43°57,994; E30°45,020	27		x	x	x	x
GAS-CS13	N43°59,298; E30°57,234	25		x	x	x	x
GAS-CS14	N43°56,361; E30°51,044	22		x	x	x	x
GAS-CS16	N43°55,450; E30°45,427	30			x	x	x
GAS-CS18	N43°55,777; E30°45,301	30			x	x	x
GAS-IS01	N43°57,378; E30°46,012	13		x	x	x	x
GAS-IS03	N43°57,156; E30°45,082	6		x	x	x	x
GAS-IS05	N43°58,3944; E30°59,7349	8		x	x	x	x
GAS-IS09	N44°05,191; E30°47,966	5		x	x	x	x
GAS-IS12	N43°55,540; E30°45,299	12			x	x	x
	Sum:	377					

Table 17: List of cores recovered and sampled for pore-fluid analyses

Core GAS-CS01

GAS-CS01	S02	108	GAS-CS01	S19	1795
GAS-CS01	S02	183	GAS-CS01	S19	1820
GAS-CS01	S02	158	GAS-CS01	S19	1845
GAS-CS01	S03	207	GAS-CS01	S20	1920
GAS-CS01	S03	266	GAS-CS01	S20	1895
GAS-CS01	S03	281	GAS-CS01	S20	1945
GAS-CS01	S04	307	GAS-CS01	S21	1995
GAS-CS01	S04	332	GAS-CS01	S21	2020
GAS-CS01	S04	382	GAS-CS01	S21	2045
GAS-CS01	S05	407	GAS-CS01	S22	2095
GAS-CS01	S05	457	GAS-CS01	S22	2120
GAS-CS01	S05	482	GAS-CS01	S22	2145
GAS-CS01	S06	557	GAS-CS01	S23	2195
GAS-CS01	S06	582	GAS-CS01	S23	2271
GAS-CS01	S06	507	GAS-CS01	S23	2221
GAS-CS01	S07	607	GAS-CS01	S24	2319
GAS-CS01	S07	657	GAS-CS01	S24	2345
GAS-CS01	S07	682	GAS-CS01	S24	2295
GAS-CS01	S08	702	GAS-CS01	S25	2395
GAS-CS01	S08	757	GAS-CS01	S25	2421
GAS-CS01	S08	732	GAS-CS01	S25	2442
GAS-CS01	S09	793	GAS-CS01	S26	2495
GAS-CS01	S09	882	GAS-CS01	S26	2520
GAS-CS01	S09	859	GAS-CS01	S26	2570
GAS-CS01	S10	907	GAS-CS01	S27	2589
GAS-CS01	S10	983	GAS-CS01	S27	2639
GAS-CS01	S10	932	GAS-CS01	S27	2664
GAS-CS01	S12	1107	GAS-CS01	S28	2689
GAS-CS01	S12	1132	GAS-CS01	S28	2714
GAS-CS01	S12	1157	GAS-CS01	S28	2739
GAS-CS01	S13	1207	GAS-CS01	S29	2789
GAS-CS01	S13	1257	GAS-CS01	S29	2824
GAS-CS01	S13	1282	GAS-CS01	S29	2849
GAS-CS01	S14	1308	GAS-CS01	S30	2948
GAS-CS01	S14	1333	GAS-CS01	S30	2904
GAS-CS01	S14	1372	GAS-CS01	S30	2865
GAS-CS01	S15	1407	GAS-CS01	S31	3045

GAS-CS01	S15	1432	GAS-CS01	S31	2970
GAS-CS01	S15	1457	GAS-CS01	S31	3008
GAS-CS01	S16	1570	GAS-CS01	S32	3080
GAS-CS01	S16	1495	GAS-CS01	S32	3112
GAS-CS01	S16	1520	GAS-CS01	S32	3145
GAS-CS01	S17	1620	GAS-CS01	S33	3180
GAS-CS01	S17	1595	GAS-CS01	S33	3240
GAS-CS01	S17	1630	GAS-CS01	S33	3215
GAS-CS01	S18	1720	GAS-CS01	S34	3315
GAS-CS01	S18	1745	GAS-CS01	S34	3280
GAS-CS01	S18	1695	GAS-CS01	S34	3330

Core GAS-CS03

GAS-CS03	S01	30	GAS-CS03	S13	1263
GAS-CS03	S01	75	GAS-CS03	S14	1308
GAS-CS03	S02	120	GAS-CS03	S14	1358
GAS-CS03	S02	170	GAS-CS03	S15	1377
GAS-CS03	S02	180	GAS-CS03	S15	1442
GAS-CS03	S03	220	GAS-CS03	S16	1642
GAS-CS03	S03	270	GAS-CS03	S16	1558
GAS-CS03	S04	320	GAS-CS03	S16	1582
GAS-CS03	S04	370	GAS-CS03	S16	1667
GAS-CS03	S05	420	GAS-CS03	S17	1558
GAS-CS03	S05	475	GAS-CS03	S17	1582
GAS-CS03	S06	570	GAS-CS03	S18	1642
GAS-CS03	S06	520	GAS-CS03	S18	1667
GAS-CS03	S07	620	GAS-CS03	S19	1790
GAS-CS03	S07	670	GAS-CS03	S19	1767
GAS-CS03	S08	720	GAS-CS03	S20	1817
GAS-CS03	S08	770	GAS-CS03	S20	1867
GAS-CS03	S09	820	GAS-CS03	S21	1968
GAS-CS03	S09	870	GAS-CS03	S21	1917
GAS-CS03	S10	918	GAS-CS03	S22	2016
GAS-CS03	S10	968	GAS-CS03	S22	2041
GAS-CS03	S11	1068	GAS-CS03	S23	3014
GAS-CS03	S11	1018	GAS-CS03	S23	3067
GAS-CS03	S12	1115	GAS-CS03	S26	2217
GAS-CS03	S12	1165	GAS-CS03	S26	2232
GAS-CS03	S13	1203			

Core GAS-CS04

GAS-CS04	S01	20
GAS-CS04	S01	45
GAS-CS04	S02	82
GAS-CS04	S02	132
GAS-CS04	S03	164
GAS-CS04	S03	222
GAS-CS04	S04	274
GAS-CS04	S04	324
GAS-CS04	S05	374
GAS-CS04	S05	424
GAS-CS04	S06	474
GAS-CS04	S06	524

Core GAS-CS07

GAS-CS07	S02	120
GAS-CS07	S02	145
GAS-CS07	S02	193
GAS-CS07	S03	220
GAS-CS07	S03	245
GAS-CS07	S03	295
GAS-CS07	S04	385
GAS-CS07	S04	320
GAS-CS07	S04	355
GAS-CS07	S05	407
GAS-CS07	S05	455
GAS-CS07	S06	521
GAS-CS07	S06	555
GAS-CS07	S07	623
GAS-CS07	S07	687

GAS-CS07	S08	720
GAS-CS07	S08	745
GAS-CS07	S08	789
GAS-CS07	S10	915
GAS-CS07	S10	940
GAS-CS07	S10	990
GAS-CS07	S11	1015
GAS-CS07	S11	1040
GAS-CS07	S11	1075
GAS-CS07	S12	1117
GAS-CS07	S12	1138

Core GAS-CS12

GAS-CS12	S02a	0,64	GAS-CS12	S14	12,95
GAS-CS12	S02c	1,14	GAS-CS12	S14	13,38
GAS-CS12	S03	1,65	GAS-CS12	S15	13,7
GAS-CS12	S03	2,15	GAS-CS12	S15	14,34
GAS-CS12	S04b	2,94	GAS-CS12	S16a	14,87
GAS-CS12	S04b	3,4	GAS-CS12	S17	15,84
GAS-CS12	S05c	4,09	GAS-CS12	S17	16,34
GAS-CS12	S06c	5,14	GAS-CS12	S18	16,59
GAS-CS12	S06c	5,64	GAS-CS12	S18	17,09
GAS-CS12	S07a	6,34	GAS-CS12	S19	17,36
GAS-CS12	S08	6,95	GAS-CS12	S19	17,59
GAS-CS12	S09	7,64	GAS-CS12	S20a	17,91
GAS-CS12	S11	9,7	GAS-CS12	S21	18,92
GAS-CS12	S11	9,95	GAS-CS12	S21	19,67
GAS-CS12	S11	10,2	GAS-CS12	S22	19,92
GAS-CS12	S11	10,45	GAS-CS12	S22	20,68
GAS-CS12	S12	10,65	GAS-CS12	S23	21,12
GAS-CS12	S12	10,89	GAS-CS12	S23	21,62
GAS-CS12	S12c		GAS-CS12	S24	21,97
GAS-CS12	S13a	11,7	GAS-CS12	S24	22,54
GAS-CS12	S13a	12,08			

Core GAS-CS13

GAS-CS13	S01	20	GAS-CS13	S09	801
GAS-CS13	S01	70	GAS-CS13	S09	801
GAS-CS13	S02	114	GAS-CS13	S10	828
GAS-CS13	S02	191	GAS-CS13	S10	853
GAS-CS13	S03	264	GAS-CS13	S10	853
GAS-CS13	S04	366	GAS-CS13	S10	878
GAS-CS13	S05	431	GAS-CS13	S10	903
GAS-CS13	S05	471	GAS-CS13	S10	903
GAS-CS13	S06	512	GAS-CS13	S11	928
GAS-CS13	S06	540	GAS-CS13	S11	953
GAS-CS13	S06	581	GAS-CS13	S11	953
GAS-CS13	S07	641	GAS-CS13	S11	975
GAS-CS13	S07	691	GAS-CS13	S12	1028
GAS-CS13	S08	719	GAS-CS13	S12	1053
GAS-CS13	S08	739	GAS-CS13	S12	1078
GAS-CS13	S08	739	GAS-CS13	S13	1093
GAS-CS13	S08	769	GAS-CS13	S13	1125

Core GAS-CS14

GAS-CS14	S01	21
GAS-CS14	S01	47
GAS-CS14	S01	9
GAS-CS14	S02	57
GAS-CS14	S02	78
GAS-CS14	S02	97
GAS-CS14	S03	110
GAS-CS14	S03	148
GAS-CS14	S03	178
GAS-CS14	S03	198
GAS-CS14	S04	218
GAS-CS14	S04	238
GAS-CS14	S06	244
GAS-CS14	S06	244
GAS-CS14	S06	244

GAS-CS14	S07	305
GAS-CS14	S07	305
GAS-CS14	S07	305

Core GAS-IS12

GAS-IS12	S01	3,5
GAS-IS12	S01	19,5
GAS-IS12	S01	27,5
GAS-IS12	S02	32,5
GAS-IS12	S02	43,5
GAS-IS12	S02	52,5

Table 18: List of cores sampled for XRF and XRD analyses

- Sample splits for onshore measurements

Samples were split for post-cruise analyses either for Kiel (Geomar) or for Brest (Ifremer). Aliquots of pore-fluid for postcruise analyses in Kiel included an acidified aliquot. Aliquots of pore-fluid for post-cruise analyses in Brest (Ifremer) included samples stored in pre-evacuated and sealed vials, samples stored in acidified vial (10 µL of HNO₃ ultrapure- Ultrex). These samples were used onshore for major (Cl, SO₄, Br, I, Na, K, Ca, Mg) and minor (Sr, Li, B, Ba, Mn) element analyses by ionic chromatography and HR-ICP-MS, respectively; and δ¹³C-CH₄, strontium and possibly lithium isotope measurements by MC-ICP-MS.

- Alkalinity measurement

The total alkalinity (A_T) of the pore fluid is its ability to absorb ions H⁺. It is expressed as the sum of the concentration of several anions such as:

$$A_T = [\text{HCO}_3^-] + 2 [\text{CO}_3^{2-}] + [\text{B}(\text{OH})_4^-] + [\text{OH}^-] + [\text{SiO}(\text{OH})_3^-] + \dots$$

where:

HCO₃⁻ and CO₃²⁻ are carbonate ions
 B(OH)₄⁻ is borate ion
 OH⁻ is hydroxyl ion
 SiO(OH)₃⁻ is silicate ion

In the present study, the alkalinity was directly measured after sampling by using a titrimeter and a solution of HCl 0.1M. 150 µL of sample was put into a titration cell. The HCl was added stepwise using an automatic burette with an increment of 0.001mL.

The value of the alkalinity was calculated at the equivalent point (EP) using the following relationship:

$$\text{Alkalinity } / \mu\text{M} = ((V_1 * C_1) / V_2) * 1000$$

where:

V₁ is the volume of sample
 V₂ is the volume of HCl added
 C₁ is the concentration of HCl (here 0,1M)

The pH value of the pore-fluid samples was measured at the beginning of each alkalinity measurement.

- Chloride and sulfate measurements

Besides the titration for alkalinity, the samples were also analysed for sulfate and chloride concentration determination using a Dionex® ICS-2000 instrument equipped with an autosampler from the Laboratoire de Géochimie et Métallogénie, Unité des Geosciences Marines, IFREMER. A Ionpac AS-17C column of 250 mm in length and 4 mm in diameter equipped with a 4 mm ASRS suppressor was used. The detection limits were 1.5 ppm and 5 ppm for sulfate and chloride, respectively.

VIII. REFERENCES

- Bhatnagar, G., Chapman, W.G., Dickens, G.R., Dugan, B., Hirasaki, G.J., 2008. Sulfate-methane transition as a proxy for average methane hydrate saturation in marine sediments. *Geophysical Research Letters*, 35(3).
- Bhatnagar, G. et al., 2011. Analytical theory relating the depth of the sulfate-methane transition to gas hydrate distribution and saturation. *Geochemistry Geophysics Geosystems*, 12.
- Boetius, A. et al., 2000. A marine microbial consortium apparently mediating anaerobic oxidation of methane. *Nature*, 407(6804): 623-626.
- Borowski, W.S., Paull, C.K., Ussler, W., 1996. Marine pore-water sulfate profiles indicate in situ methane flux from underlying gas hydrate. *Geology*, 24(7): 655-658.
- Bourillet J-F., de Chambure L., Loubrieu B. and Guillaumont B. (2011). Geomorphological classification of cold water coral seabed (Bay of Biscay – NE Atlantic). The Geohab 2011 conference, Marine geological and biological habitat mapping, 3-6 May, Espoo, Geological Survey of Finland.
- Chand, S., T. A. Minshull, D. Gei, and J. M. Carcione (2004), Elastic velocity models for gas hydrate-bearing sediments: A comparison, *Geophys. J. Int.*, 159(2), 573–590.
- Chand, S., T. A. Minshull, J. A. Priest, A. I. Best, C. R. I. Clayton, and W. F. Waite (2006), An effective medium inversion algorithm for gas hydrate quantification and its application to laboratory and borehole measurements of gas hydrate-bearing sediments, *Geophys. J. Int.*, 166(2), 543–552.
- Dallimore, S.R., Wright, J.F., Nixon, F.M., Kurihara, M., Yamamoto, K., Fujii, T., Fujii, K., Numasawa, M., Yasuda, M., Imasato, Y., 2008. Geologic and Porous Media Factors Affecting the 2007 Production Response Characteristics of the JOGMEC/NRCan/Aurora Mallik Gas Hydrate Production Research Well. Proceedings of the 6th International Conference on Gas Hydrates, Vancouver, Canada.
- De Chambure L. and Bourillet J-F. (2010). Geomorphological classification of the seabed - Bay of Biscay CoralFISH 2nd science meeting 29th November - 2nd December 2010, Milan, Italy.
- De Chambure L. and Bourillet J-F. (2011). Geomorphological classification in Bay of Biscay - CoralFISH project WP1. Ifremer. Brest, France, rapport interne GM/LES 2011, Ifremer.
- Froelich, P.N. et al., 1979. Early oxidation of organic matter in pelagic sediments of the eastern equatorial Atlantic: suboxic diagenesis. *Geochimica et Cosmochimica Acta*, 43(7): 1075-1090.
- Gregoire, M., Raick, C., Soetaert, K., 2008. Numerical modeling of the deep black sea ecosystem functioning during the late 1980s (eutrophication phase). *Progress in Oceanography* 76, 286–333.
- Helgerud, M. B., J. Dvorkin, A. Nur, A. Sakai, and T. Collett (1999), Elastic wave velocity in marine sediments with gas hydrates: Effective medium modeling, *Geophys. Res. Lett.*, 26(13), 2021–2024.
- Jakobsen, M., J. A. Hudson, T. A. Minshull, and S. C. Singh (2000), Elastic properties of hydrate-bearing sediments using effective medium theory, *J. Geophys. Res.*, 105(B1), 561–577.

Joye, S.B. et al., 2004. The anaerobic oxidation of methane and sulfate reduction in sediments from Gulf of Mexico cold seeps. *Chemical Geology*, 205(3-4): 219-238.

Ker, S., Marsset, B., Garziglia, S., Le Gonidec, Y., Gibert, D., Voisset & M., Adamy, J., 2010. High-resolution seismic imaging in deep sea from a joint deep-towed/OBH reflection experiment: application to a Mass Transport Complex offshore Nigeria, *Geophys. J. Int.*, 182, 1524-1542.

Klaucke, I., Sahling, H., Weinrebe, W., Blinova, V., Burk, D., Lursmanashvili, N., and Bohrmann, G., 2006. Acoustic investigation of cold seeps offshore Georgia, eastern Black Sea, *Mar. Geol.*, 231, 51–67.

Kruglyakova, R.P., Byakov, Y.A., Kruglyakova, M.V., Chalenko, L.A. and Shevtsova, N.T., 2004. Natural oil and gas seeps on the Black Sea floor. *Geo-Marine Letters*, 24(3): 150-162.

Kuşçu, I., Okamura, M., Matsuoka, H., Gokasan, E., Awata, Y., Tur, H., Simsek, M., 2005. Seafloor gas seeps and sediment failures triggered by the August 17, 1999 earthquake in the Eastern part of the Gulf of Izmit, Sea of Marmara, NW Turkey. *Mar. Geol.* 215, 193–214.

Kvenvolden, K. A.: "Natural gas hydrate occurrence and issues.", *Ann. N.Y. Acad. Sci.* (1994), 715, 232.

Lee, M. W., D. R. Hutchinson, T. S. Collett, and W. P. Dillon (1996), Seismic velocities for hydrate-bearing sediments using weighted equation, *J. Geophys. Res.*, 101(B9), 20,347–20,358.

Lericolais, G., J. Bourget, I. Popescu, P. Jermannaud, T. Mulder, S. Jorry, N. Panin, 2012. Late Quaternary deep-sea sedimentation in the western Black Sea: New insights from recent coring and seismic data in the deep basin, *Global and Planetary Change*, 10.1016/j.gloplacha.2012.05.002.

Ludmann, T., Wong, H.K., Konerding, P., Zillmer, M., Petersen, J. and Fluh, E., 2004. Heat flow and quantity of methane deduced from a gas hydrate field in the vicinity of the Dnieper Canyon, northwestern Black Sea. *Geo-Marine Letters*, 24(3): 182-193.

Marsset, T., Marsset, B., Ker, S., Thomas, Y. & Le Gall, Y., 2010. High and very high resolution deep-towed seismic system: Performance and examples from deepwater Geohazard studies. *Deep-Sea Research I*.

Masuda Y., Yamamoto K., Shimada T., Ebinuma T. and Nagakubo S., 2009. Japan's Methane Hydrate R&D Program Progresses to Phase 2. *Fire in the Ice*. Volume 9, Issue 4.

Masui, A., Haneda, H., Ogata, Y., Aoki, K. 2005. Effects of methane hydrate formation on shear strength of synthetic methane hydrate sediments. In: *Proceedings of the 15th International Offshore and Polar Engineering Conference*, Seoul, p. 364-369.

Masui, A., Miyazaki, K., Haneda, H., Ogata, Y., Aoki, K. 2008. Mechanical characteristics of natural and artificial gas hydrate bearing sediments. In : *Proceedings of the 6th International Conference on Gas Hydrates*, Vancouver.

Mclver, R. D.: "Role of naturally occurring gas hydrates in sediment transport.", *American Association of Petroleum Geologists Bulletin* (1982), 66, 789.

Meister, P., Liu, B., Ferdelman, T.G., Jørgensen, B.B., Khalili, A., 2013. Control of sulphate and methane distributions in marine sediments by organic matter reactivity. *Geochimica et Cosmochimica Acta*, 104: 183-193.

Naudts, L., Greinert, J., Artemov, Y., Staelens, P., Poort, J., Van Rensbergen, P. and De Batist, M., 2006. Geological and morphological setting of 2778 methane seeps in the Dnepr paleo-delta, northwestern Black Sea. *Marine Geology*, 227(3-4): 177-199.

Niewohner, C., Hensen, C., Kasten, S., Zabel, M., Schulz, H.D., 1998. Deep sulfate reduction completely mediated by anaerobic methane oxidation in sediments of the upwelling area off Namibia. *Geochimica et Cosmochimica Acta*, 62(3): 455-464.

Nikolovska, A., Sahling, H., Bohrmann, G., 2008. Novel hydro-acoustic methodology for detection, localization and quantification of gas bubbles rising from the seafloor at cold seeps. *Geochemistry Geophysics Geosystems* 9, Q10010, doi:10.1029/2008GC002118.

Oguz, T., A.G. Deshpande, P. Malanotte-Rizzoli, 2002. The rôle of mesoscale processes controlling biological variability in the Black Sea coastal waters: inferences from SeaWiFS-derived surface chlorophyll field. *Continental Shelf Research* 22, 1477-1492.

Orcutt, B.N. et al., 2004. Life at the edge of methane ice: microbial cycling of carbon and sulfur in Gulf of Mexico gas hydrates. *Chemical Geology*, 205(3-4): 239-251.

Özsoy, E., Unluata, U., Top, Z., 1993. The evolution of Mediterranean water in the Black Sea: interior mixing and material transport by double diffusive intrusions. *Progress in Oceanography* 31, 275–320.

Pape, T., Blumenberg, M., Seifert, R., Bohrmann, G. and Michaelis, W., 2008. Marine Methane Biogeochemistry of the Black Sea: A Review. In: Y.F.H.M.K. Dilek (Editor), *Links between Geological Processes, Microbial Activities & Evolution of Life: Microbes and Geology. Modern Approaches in Solid Earth Sciences*, pp. 281-311.

Plaza-Faverola Andreia, Westbrook Graham K., Ker Stephan, Exley Russell J. K., Gailler Audrey, Minshull Tim A., Broto Karine (2010). Evidence from three-dimensional seismic tomography for a substantial accumulation of gas hydrate in a fluid-escape chimney in the Nyegga pockmark field, offshore Norway. *Journal Of Geophysical Research-solid Earth*, 115(B08104), 1-24.

Pohlman, J.W., Ruppel, C., Hutchinson, D.R., Downer, R., Coffin, R.B., 2008. Assessing sulfate reduction and methane cycling in a high salinity pore water system in the northern Gulf of Mexico. *Marine and Petroleum Geology*, 25(9): 942-951.

Popescu, I., De Batist, M., Lericolais, G., Nouze, H., Poort, J., Panin, N., Versteeg, W. and Gillet, H., 2006. Multiple bottom-simulating reflections in the Black Sea: Potential proxies of past climate conditions. *Marine Geology*, 227(3-4): 163-176.

Popescu, I., Lericolais, G., Panin, N., De Batist, M. and Gillet, H., 2007. Seismic expression of gas and gas hydrates across the western Black Sea. *Geo-Marine Letters*, 27(2-4): 173-183.

Reeburgh, W.S., 1976. Methane consumption in Cariaco Trench waters and sediments. *Earth and Planetary Science Letters*, 28(3): 337-344.

Regnier, P. et al., 2011. Quantitative analysis of anaerobic oxidation of methane (AOM) in marine sediments: A modeling perspective. *Earth-Science Reviews*.

Ruffine, L., Caprais, J.L., Bayon, G., Riboulot, V., Donval, J.P., Etoubleau, J., Birot, D., Pignet, P., Rongemaille, E., Chazallon, B., Grimaud, S., Adamy, J., Charlou, J.L. and Voisset, M., 2012a. Investigation on the geochemical dynamics of a hydrate-bearing pockmark in the Niger Delta. *Marine and Petroleum Geology*, Submitted.

Ruffine, L., Fandino, O., Etoubleau, J., Chéron, S., Donval, J.P., Germain, Y., Ponzevera, E., Guyader, V., Dennielou, B., Etiope, G., Gasperini, L., Bortoluzzi, G., Henry, P., Grall, C., Çagatay, M.N., Charlou, J.L. and Géli, L., 2012b. Geochemical dynamics of the natural-gas hydrate system in the Sea of Marmara, offshore Turkey. *Natural Gas*, ISBN 978-953-51-0507-7 (Advances in Natural Gas Technology): 28.

Sultan, N., De Gennaro, V., Puech, A., 2012. Mechanical behaviour of gas-charged marine plastic sediments. *Geotechnique*, in press.

Sultan, N., Garziglia, S., Colliat, J.L., 2011. Gas hydrate occurrences and seafloor deformation: investigation of strain-softening of gas-hydrate bearing sediments and its consequence in terms of submarine slope instabilities. OTC21294, 18 p.

Sultan, N., & Lafuerza, S. (2013). In situ equilibrium pore-water pressures derived from partial piezoprobe dissipation tests in marine sediments. *Canadian Geotechnical Journal*, 50(12), 1294-1305.

Sultan, N., Marsset, B., Ker, S., Marsset, T., Voisset, M., Vernant, A. M., ... & Drapeau, D. (2010). Hydrate dissolution as a potential mechanism for pockmark formation in the Niger delta. *Journal of Geophysical Research: Solid Earth* (1978–2012), 115(B8).

Sultan, N., V. Riboulot, S. Ker, B. Marsset, L. Géli, J.B. Tary, F. Klingelhoefer, M. Voisset, V. Lanfumey, J.L. Colliat, J. Adamy, S. Grimaud, 2011-b. Dynamics of fault-fluid-hydrate system around a shale-cored anticline in deepwater Nigeria. *J. Geophys. Res – Solid Earth*, DOI: 10.1029/2011JB008218.

Sultan, N., Voisset, M., Marsset, T., Vernant, A. M., Cauquil, E., Colliat, J. L., & Curinier, V. (2007). Detection of free gas and gas hydrate based on 3D seismic data and cone penetration testing: An example from the Nigerian Continental Slope. *Marine Geology*, 240(1), 235-255.

Top, Z., Östlund, G., Pope, L., Grall, C., 1991. Helium isotopes, neon and tritium in Black Sea, a comparison with the 1975 observation. *Deep-Sea Res.* 38 (Suppl. 2), S747–S759.

Torres, M.E., Teichert, B.M.A., Trehu, A.M., Borowski, W., Tomaru, H., 2004. Relationship of pore water freshening to accretionary processes in the Cascadia margin: Fluid sources and gas hydrate abundance. *Geophysical Research Letters*, 31(22).

Wallmann, K. et al., 2006. Kinetics of organic matter degradation, microbial methane generation, and gas hydrate formation in anoxic marine sediments. *Geochimica et Cosmochimica Acta*, 70(15): 3905-3927.

Wallmann, K. Bialas, J. (2009). SUGAR (submarine gas hydrate reservoirs) *Environmental Earth Sciences*, 59 (2). pp. 485-487. DOI 10.1007/s12665-009-0235-x.

Westbrook, G.K., Thatcher, K.E., Rohling, E.J., et al., 2009. Escape of methane gas from the seabed along the West Spitsbergen continental margin, *Geophys. Res. Lett.*, 36, L15608.

Wilson M.F.J., O'Connell B., Brown C., Guinan J.C. and Grehan A.J. (2007). "Multiscale terrain analysis of multibeam bathymetry data for habitat mapping on the continental slope." *Marine Geodesy* 30(1): 3-35.

Zillmer, M., Flueh, E.R. and Petersen, J., 2005. Seismic investigation of a bottom simulating reflector and quantification of gas hydrate in the Black Sea. *Geophysical Journal International*, 161(3): 662-678.